POLITECNICO DI TORINO

Master's Degree in Engineering and Management

Master's Degree Thesis

Feasibility study on the use of satellite data for the construction and operation of offshore wind power plants in southeast Brazil

Gabriela Vasconcelos Araujo

Supervised by
Prof. Dr. Afonso Pagani
Prof. Dr. Demétrio Cornilios Zachariadis

July 2024

Summary

The aim of this graduation thesis is to develop a feasibility study on the use of satellite data for the construction and operation of offshore wind power plants in southeast Brazil as a way to further diversify the Brazilian energy matrix. In order to do that, the environmental licensing process in Brazil is reviewed, followed by a technology analysis comprising data collection and wind monitoring, as well as a study of the main wind parameters considered in site selection for a power plant, including wind speed, wind direction, load analysis, turbulence intensity and wind shear. Subsequently, a brief analysis of an article from bibliography was made around the wind speed trends and the potential of electricity generation at new wind power plants in northeast Brazil. Lastly, a study case was conducted once a study area was defined, utilizing data collected by ESA's Aeolus satellite in 2022, on an area equivalent to a polygon with longitudes ranging from -42.1736 to -50.4697 and latitudes from -22.4105 to -27.072, a coastal region in southeast Brazil. Based on wind speed and its distribution, the total power output for one single turbine SG 14-222 DD was estimated in 17,507.30 MWh/year. In conclusion, the use of Aeolus data to determine the feasibility of the construction and operation of wind power plants proved to be a valuable tool in the decision-making process, in particular when aligned with on site measurements.

Keywords: offshore wind power, wind turbines, wind velocity, southeast Brazil, energy diversification, environmental licensing, satellite data collection, data analysis.

Acknowledgements

I would like to express my deepest gratitude to my dedicated supervisors, Prof. Dr. Afonso Pagani, Prof. Dr. Demétrio Cornilios Zachariadis and Marianna Valente, for their valuable guidance, expertise, and constructive feedback that significantly contributed to the success of this study, through all the stages of writing my project.

Special appreciation also goes to my family and boyfriend, to whom I express my deepest gratitude for their support throughout this academic pursuit. Their encouragement has been a constant source of motivation and inspiration.

Additionally, I extend my appreciation to all my friends and colleagues with whom I have shared this important and memorable cycle of my life. I look forward to the next step.

Table of Contents

List of Tables

List of Figures

Acronyms

IBAMA
Instituto Brasileiro do Meio Ambiente e dos Recursos Naturais Renováveis

TR
Termo de Referência (*Terms of Reference*)

EIA
Estudo de Impacto Ambiental *(Environmental Impact Study)*

Rima
Relatório de Impacto Ambiental (*Environmental Impact Report*)

EUSPA
European Union Agency for the Space Program

EO
Earth Observation

IMF
International Monetary Fund

EPE
Empresa de Pesquisa Energética

NOAA
National Oceanic and Atmospheric Administration

INPE
Instituto Nacional de Pesquisas Espaciais (*National Institute for Space Research*)

CBERS

China-Brazil Earth Resources Satellite Program

GOES

Geostationary Operational Environmental Satellites

EUMETSAT

European Organisation for the Exploitation of Meteorological Satellites

NASA

National Aeronautics and Space Administration

MODIS

Moderate Resolution Imaging Spectroradiometer

JAXA

Japan Aerospace Exploration Agency

OB.DAAC

cean Biology Distributed Active Archive Center

EOSDIS

Earth Observing System Data and Information System

SST

Sea Surface Temperature

GCOM-W1

Global Change Observation Mission - Water

CMEMS

Copernicus Marine Environment Monitoring Service

NCEI

National Centers for Environmental Information

CCI

Climate Change Initiative

USGS

United States Geological Survey

SRTM

Shuttle Radar Topography Mission

ASTER

Advanced Spaceborne Thermal Emission and Reflection Radiometer

VIIRS

Visible Infrared Imaging Radiometer Suite

InSAR

Interferometric Synthetic Aperture

ECMWF

European Centre for Medium-Range Weather Forecasts

VirES

Virtual Earth Explorer

UCS

Union of Concerned Scientists

HLOS

Horizontal Line of Sight

ANEEL

Agência Nacional de Energia Elétrica

Chapter 1

Introduction

In the pursuit of sustainable and renewable energy sources, offshore wind power has emerged as a significant player in the global energy landscape. With its potential to harness strong and consistent winds over open seas, offshore wind power plants have gained importance as a viable alternative to conventional energy sources, contributing to both environmental preservation and energy security. Nevertheless, its current development, specially in Brazil, is still limited by both its newness and licensing process. In order to further develop a feasibility study on the usage of satellite data for the construction and operation of offshore wind power plants in southeast Brazil, it is necessary to first understand the concepts surrounding the theme, including both a historical overview of non renewable and renewable power sources and the current energy matrix in Brazil, as well as satellite usage for covering data specially on Earth Observation (EO).

1.1 Historical overview of the global energy matrix

Humanity's quest for energy sources has undergone a remarkable journey throughout history. As seen in Figure 1.1 and Figure 1.2, each era was characterized by distinct sources and technologies that have shaped societies and economies, based on its demands. In the pre-Industrial Revolution period, biomass in the form of wood, crop residues, and animal dung were the predominant energy source, serving the basic needs of heating, cooking, and powering small mechanical tasks. During this period, human and animal labor were fundamental sources of energy, driving sectors such as transportation, agriculture, and a limited range of industrial activities.

Following the middle ages, the turning point in energy consumption and generation was associated with the Industrial Revolution in the 18th and 19th centuries, marked by the ascendancy of coal as the primary energy source. Societies before the

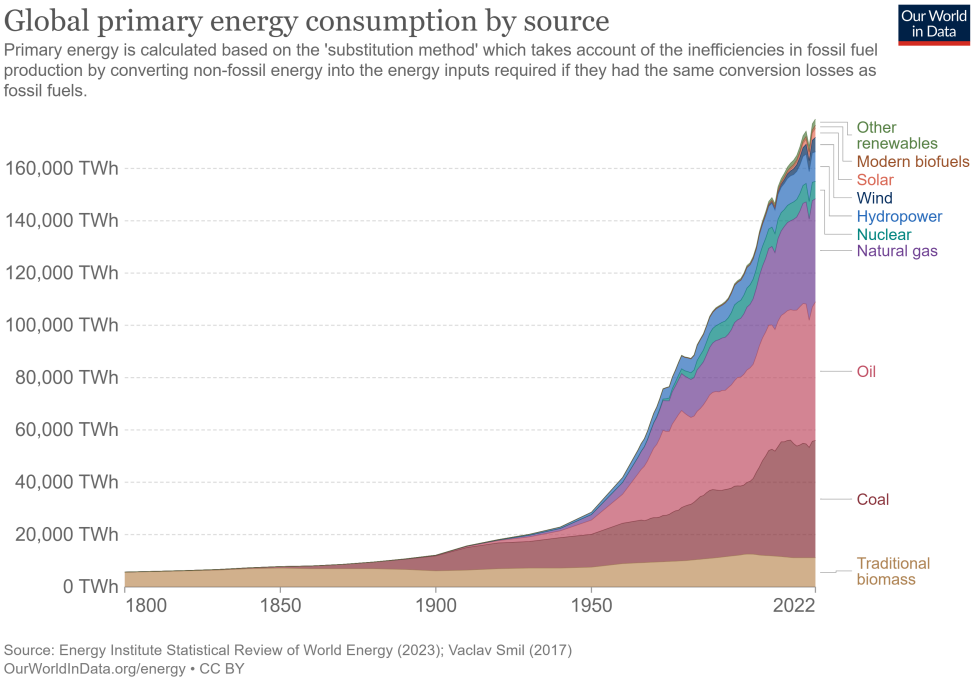

Figure 1.1: Global primary energy consumption by source

Industrial Revolution were dependent on the annual cycle of plant photosynthesis for both heat and mechanical energy. Consequently, the quantity of energy available each year was limited, and economic growth was necessarily constrained. On the other hand, in the Industrial Revolution, energy usage increased drastically, and so did the economic output. The energy source continued to be plant photosynthesis, however, accumulated over a geological age in the form of coal, a nonrenewable energy resource, once it cannot be replaced on the short term after its usage [1].

The production of thermal energy, to then generate mechanical energy, was the core driver of this transformation. Coal-fired steam engines catalyzed transformative changes in transportation, manufacturing, and agriculture, leading societies into an era of unprecedented economic growth and urbanization. In addition, this period saw the early adoption of electricity generation, utilizing coal-powered steam engines, laying the foundation for electrification.

Following the 1800s, the 20th century inaugurated the era of fossil fuels, with oil and natural gas becoming dominant sources of energy for transportation, manufacturing, and electricity generation due to their energy density and versatility. Moreover, an important transition occurred towards electricity, which became the primary form of energy for various applications. In that sense, the development of electrical grids and the electrification of homes and industries revolutionized energy

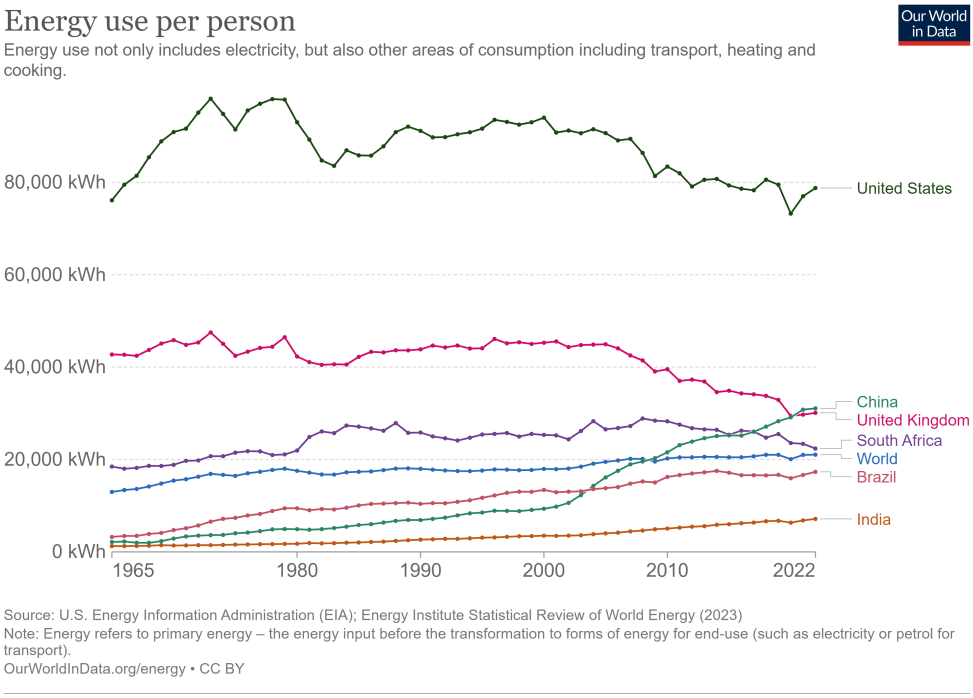

Figure 1.2: Global primary energy consumption by source

consumption, making it possible to power everything from lighting to appliances and industrial machinery. This expansion of the electricity sector was driven primarily by coal and, later in the century, natural gas, as these fossil fuels offered a reliable and efficient source of power for electric generators.

Alternatively, nuclear energy also emerged as a viable energy source in the mid-20th century, with low-carbon emission and both civilian and military applications. After World War II, governments and scientists began exploring the peaceful applications of nuclear energy. In 1951, the Experimental Breeder Reactor-I (EBR-I) in the United States became the first nuclear reactor to generate electricity. Nevertheless, this period also saw the occurrence of significant nuclear accidents, most notably the Chernobyl disaster in 1986, which led to a re-evaluation of nuclear safety standards and influenced energy policies in many countries.

At the same time, oil consumption surged due to the proliferation of the automobile and the expansion of global transportation networks. Oil became the dominant fuel for cars, trucks, ships, and airplanes, leading the oil industry to take a central role in global geopolitics. International players like the Organization of the Petroleum Exporting Countries (OPEC) have wielded significant influence in shaping the global energy landscape by controlling oil production and prices. In consequence of this scenario, several conflicts and alliances formed around access

to oil reserves, since only a few countries have access to it, as shown in Figure 1.3. Additionally, Figure 1.4 indicates the oil quantities available in each country.

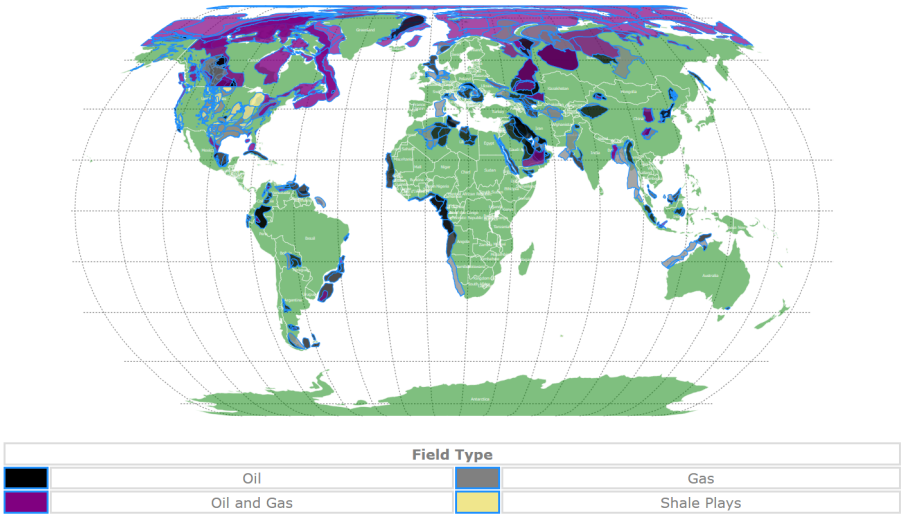

Figure 1.3: Oil reserves around the world by field [2]

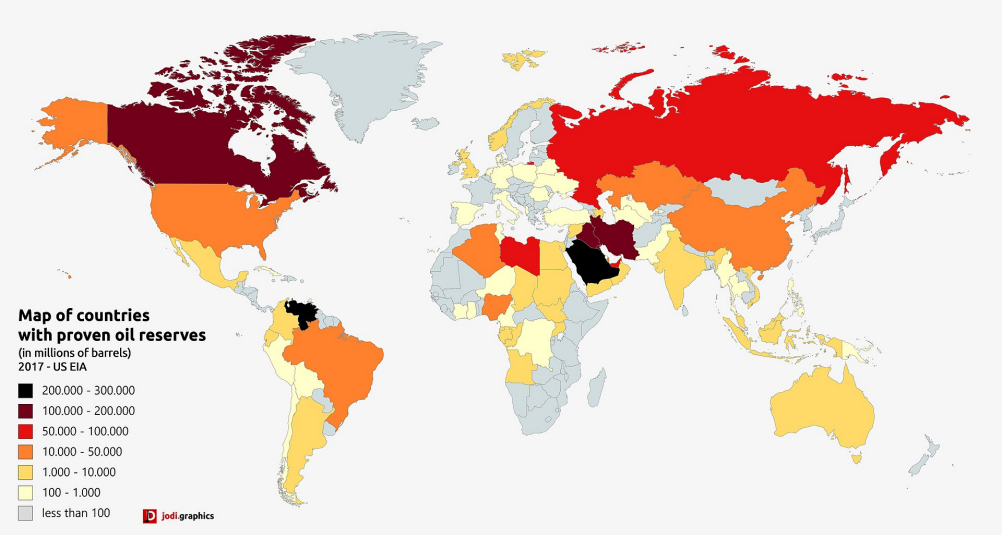

Figure 1.4: Map of countries with proven oil reserves according to U.S. EIA [3]

As the world faced issues associated with climate change and environmental degradation in the late 20th century and into the 21st century, there was a discernible shift toward renewable energy sources. Hydropower, which had been used for electricity generation since the early 20th century, gained prominence as a renewable

energy source. Wind power, driven by the development of wind turbines in the late 20th century, grew into a significant clean energy contributor. Photovoltaic solar panels, initially commercialized in the mid-20th century, experienced explosive growth in recent decades, as seen in Figure 1.1. Biomass and biofuels also found application in electricity generation and transportation.

Countries are currently at various stages of transitioning their energy matrices from fossil fuels to renewables, as shown in Figure 1.5, reflecting diverse commitments and success levels. International agreements, such as the Paris Agreement on climate change, have established frameworks for global cooperation in reducing greenhouse gas emissions and promoting renewable energy.

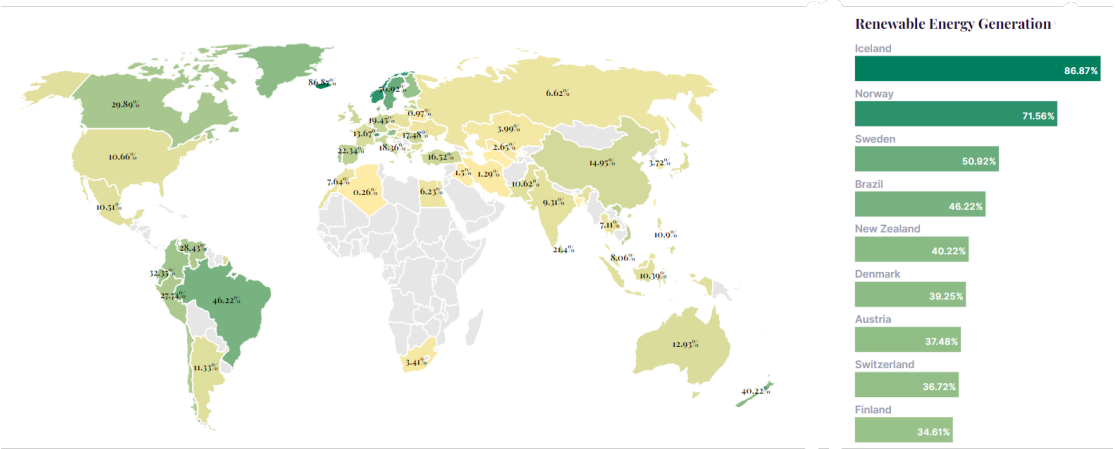

Figure 1.5: Renewable energy generation per country [4]

Once contemporary energy challenges are defined by climate change mitigation as well as environmental sustainability, energy efficiency measures are being adopted across sectors to reduce consumption. Electrification, especially in transportation and heating, is being explored to decrease dependence on fossil fuels. Renewable energy infrastructure investments, such as wind, solar, and hydropower, are being made to transition away from fossil fuels, as shown in 1.6. Looking towards the future, the global energy matrix continues to evolve, with an increasing emphasis on sustainability, energy security, and reducing the environmental impact of energy production and consumption.

1.2 Usage of satellite data for earth observation and data collection

According to the European Union Agency for the Space Program (EUSPA), Earth Observation (EO) refers to the use of remote sensing technologies to monitor

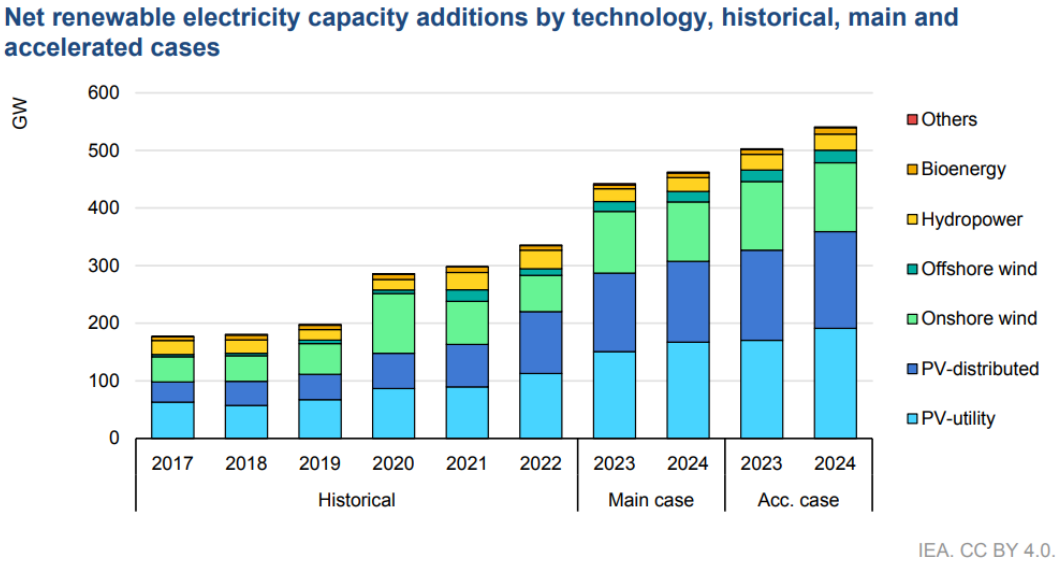

Figure 1.6: Renewable energy generation per country [5]

land, marine (seas, rivers, lakes) and atmosphere. Classified as one of the space sector applications, it involves the development and use of satellites and related subsystems to measure and monitor Earth, including its climate, environment and people. In that sense, satellite-based EO entails the utilization of satellite-mounted payloads to gather imaging data about the Earth's characteristics. Once processed, EO data can be assimilated into complex models in various sectors to produce information and intelligence such as forecasts, behavioural analysis and climate projections.

Satellites have played a pivotal role in the field of Earth Observation, offering an historical perspective on the planet's dynamic characteristics and environmental changes. Since the inception of satellite technology in the mid-20th century, these orbiting platforms have continuously evolved and provided scientists, researchers, and engineers with a unique vantage point from space. This trajectory of satellite-based Earth observation has both revolutionized the understanding of the Earth and significantly advanced human's capacity to address critical challenges related to climate change, natural disasters, resource management, and urban development.

The historical significance of satellite EO becomes evident through the variety of applications it has fostered. Remote sensing capabilities, facilitated by satellites, have enabled the monitoring of land cover changes, the assessment of atmospheric conditions, and the tracking of oceanic and polar phenomena. These capabilities have been instrumental in disaster management, with early warning systems for hurricanes, tsunamis, and wildfires, thereby saving countless lives. Moreover, the historical record provided by satellites has proven invaluable for long-term climate

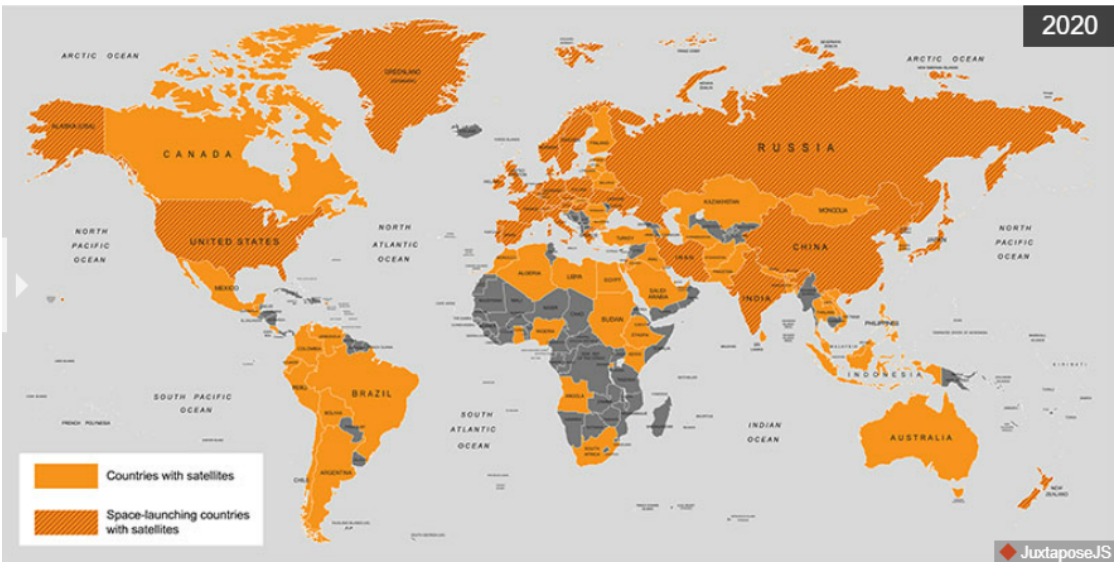

Figure 1.7: Map of countries with satellites [6]

research, aiding policymakers in understanding climate trends and supporting international climate agreements. As a result of its pivotal role in many sectors, a great number of countries now owns satellites, as shown in Figure 1.7. According to the Union of Concerned Scientists (UCS) satellite database, which lists the operational satellites in orbit on the 1st January 2023, there are 1192 EO satellites in orbit, supplying a demand that on 2021 was estimated in €536 million in revenues, as illustrated in Figure 1.8.

In the realm of engineering, satellite usage for EO has spurred technological innovation. From early, limited-resolution imagery to the deployment of advanced synthetic aperture radar (SAR) and multispectral sensors, engineers have continuously refined satellite payloads and systems to enhance data quality and coverage. This progress has resulted in smaller, more capable satellites, fostering a new era of constellations and CubeSats, which offer enhanced temporal and spatial resolution for a wide range of applications, that depends on the types of sensors on the satellite's payloads.

Optical or thermal sensors are payloads monitoring the energy received from the Earth through the reflection and re-emission of the Sun's energy by the Earth's surface or atmosphere. These sensors operate within the wavelength range spanning from the visible to the infrared portions of the electromagnetic spectrum. On the other hand, radar sensors serve as payloads that function within the longer wavelength region of the electromagnetic spectrum. Most part of these sensors actively emit energy directed towards the Earth's surface or atmosphere and subsequently capture the energy that is returned, enabling uninterrupted day

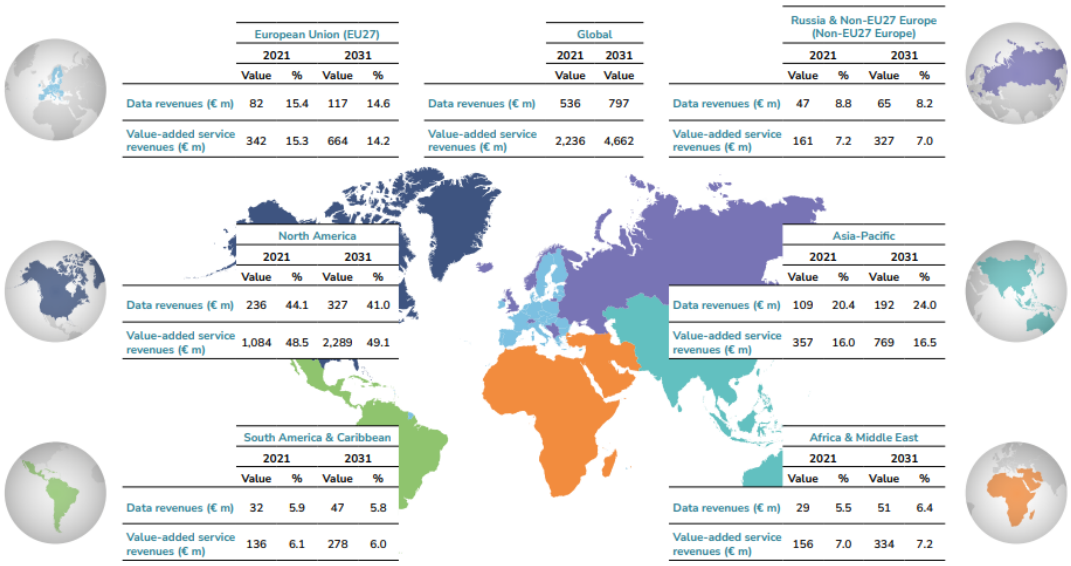

Figure 1.8: Earth Observation demand world map [7]

and night monitoring, regardless of weather conditions.

Another essential parameter in EO is the sensor resolution, divided in three different categories: spacial resolution, temporal resolution and spectral resolution. While spatial resolution defines the size of the pixels analyzed by the sensors, temporal resolution is associated with the frequency at which the data is acquired for a defined area. Lastly, spectral resolution is defined by the width of the spectrum bands. Besides sensor resolution, coverage is also a key parameter: in-orbit infrastructures offer a global coverage with a single spacecraft, while aerial or in-situ sensor coverage is local. Nevertheless, orbital geometry limits the frequency of fly-by over the same location while local monitoring allows a higher persistence, from a new acquisition every hours down to near real time.

Based on its technological characteristics, EO satellites can be applied to several market segments, ranging from the most traditional ones, like environmental monitoring, climate services, infrastructure, agriculture and aviation, to areas such as insurance and finance, cultural heritage and consumer solutions, tourism and health. Considering the scope of this project, the most relevant EO application surrounds the energy and raw materials sector, including site selection, planning and monitoring for renewable energy sources, risk management for energy assets, renewable energy assessment potential and forecast, and energy network conditions monitoring. From a global perspective, Figure 1.9 shows how the revenue from EO data and services sales are divided, with great significance given to environmental impact assessment of energy and mineral resources plant, and site selection, planning

and monitoring.

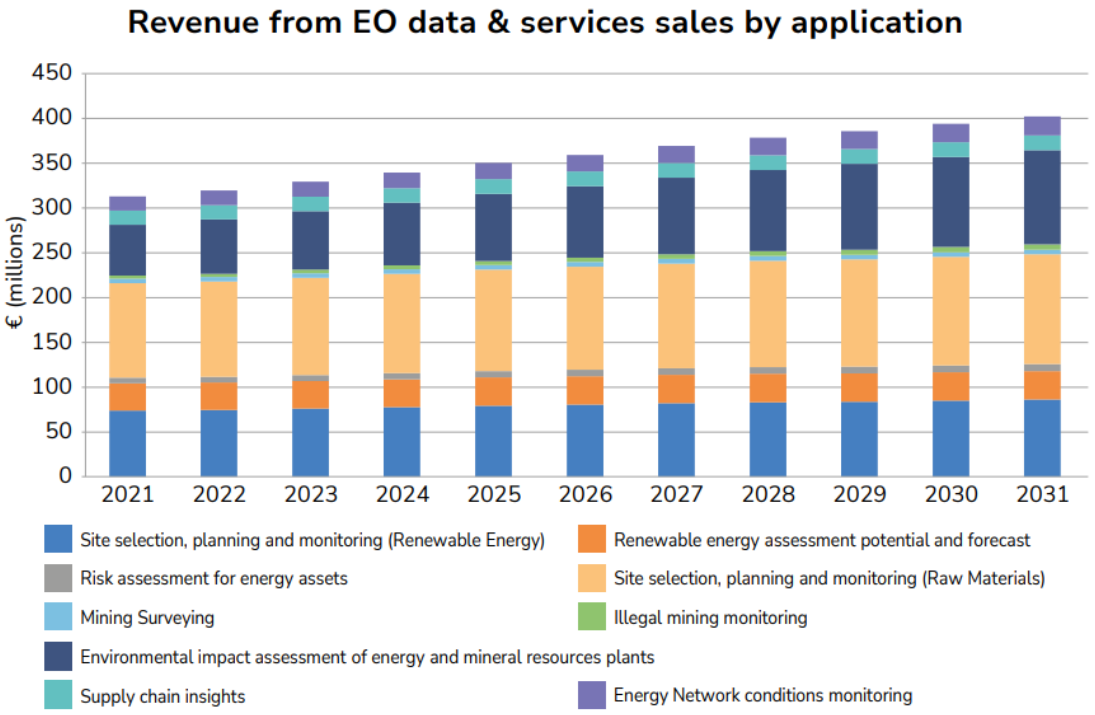

Figure 1.9: Revenue from EO data services sales by application [7]

1.3 Energy matrix in Brazil

The Brazilian energy matrix represents a complex and dynamic mix of energy sources that power 9th largest economy in the world by GDP [8]. Historically, Brazil has heavily relied on hydropower, with its abundant water resources serving as a cornerstone of the energy grid. However, the Brazilian energy matrix is experiencing a notable shift as the nation embraces renewable energy sources, including wind, solar, and biomass, as well as non-renewable sources such as natural gas and oil, as shown in Figure 1.10. This transformation is driven by a commitment to environmental sustainability, energy security, and a reduction in greenhouse gas emissions.

Brazil's electricity generation landscape is characterized by a notable reliance on hydropower, with hydropower contributing to an impressive 66% of the country's electricity demand in the year 2020. In recent years, Brazil has witnessed substantial growth in the adoption of wind and solar energy, which collectively accounted for 11% of the nation's electricity generation in the same year. Additionally, biomass

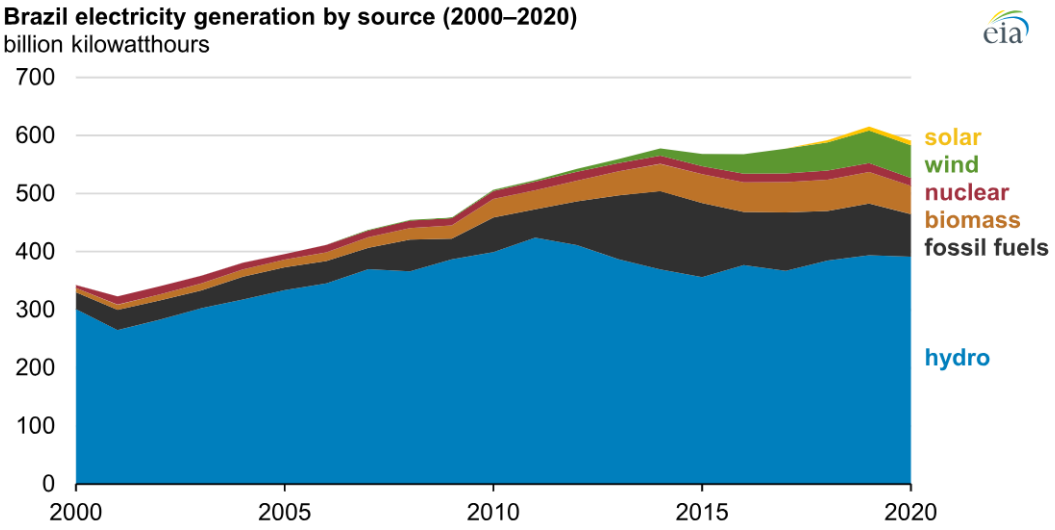

Figure 1.10: Brazil electricity generation by source [9]

constituted an 8% share in the energy matrix. Fossil fuel-fired power plants played a significant role, contributing 12% to the overall electricity generation, while nuclear power sources contributed 2%. As can be seen in Figure 1.11, renewable energy sources accounted for 47.4% of the total energy supply in 2022.

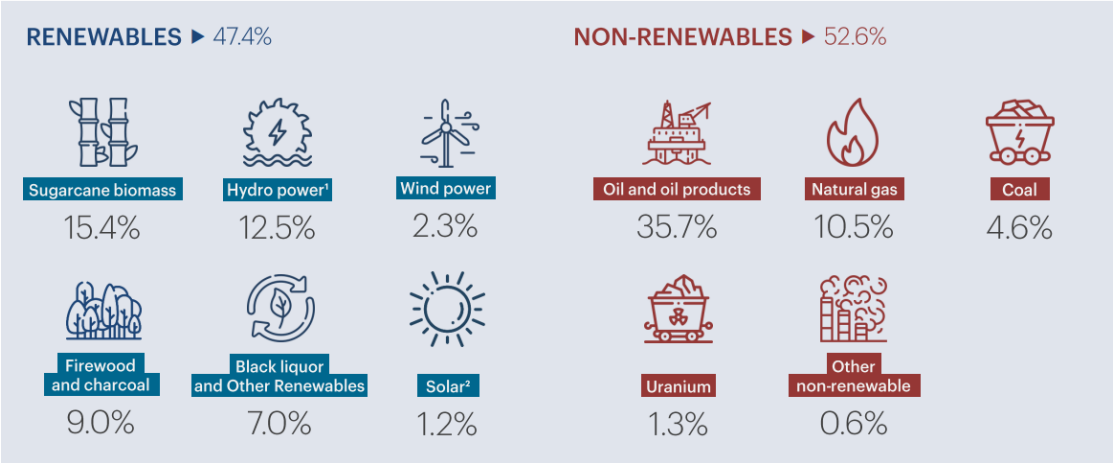

Figure 1.11: Breakdown of total energy supply in 2022 [9]

Brazil's hydropower capacity is predominantly situated in the northern regions, primarily within the Amazon River Basin. Nevertheless, the demand for electricity is predominantly concentrated along the eastern coastline, particularly in the southern regions. This geographical distribution enhances a challenge to the

nation's electricity reliability due to several factors. These include the singular reliance on hydropower, the considerable spatial separation between hydropower generation and demand centers, ongoing concerns related to drought conditions, and the consequences of deforestation. Addressing these challenges is essential to ensuring the sustainable and secure evolution of Brazil's energy landscape.

1.4 Objectives

Brazil's unique geographical and meteorological characteristics, coupled with strong government support, have positioned the country as a regional leader in renewable energy production. Nevertheless, challenges associated with studying the feasibility of the application of different renewable energy sources remain. In this project, a methodology will be proposed to study the feasibility of constructing and operating an offshore wind power plant, with a study case dedicated in using the process in southeast Brazil, based on satellite data available through ESA's Aelous program. Due to its newness, the current development of such facilities in Brazil is still limited by regulation and environmental licensing, justifying the creation of a section dedicated to understanding the current status of licensing in Brazil.

The main goal of this thesis is to present an alternative and complementary piece to in-site measurements used to evaluate the conditions for the operation of wind power plants, as well as exemplify the steps to be taken for obtaining, processing and reading open-source satellite data to perform an analysis on the construction and operation of wind power plants in a defined area.

Chapter 2

Offshore wind power plants

2.1 Overview

As already explored in Chapter 1, the escalating concerns regarding climate change and the depletion of fossil fuels have prompted a shift towards sustainable energy generation. In this context, offshore wind power plants have emerged as a promising solution due to their unique positioning in marine environments, where there is higher speed of winds, greater consistency and lack of physical interference. The market for offshore wind power has exhibited remarkable expansion over the past decade, with global installed offshore wind capacity expected to reach 630 gigawatts (GW) by 2050, up from 40 GW in 2020 [10]. More specifically, Figure 2.1 shows the expected growth divided by region, with Americas having the second biggest expected growth. This growth is attributed to advancements in turbine technology, reduced costs of installation and maintenance, and supportive policy frameworks promoting renewable energy adoption. By harnessing the immense energy potential of offshore winds, these installations offer a scalable and environmentally friendly means of meeting increasing energy demands.

In a technical way, offshore wind power operates by harnessing the kinetic energy of the wind through strategically positioned turbines at sea. These turbines, equipped with rotor blades connected to generators, initiate the energy conversion process. As the blades rotate, they turn the generator, transforming kinetic energy into electrical energy. The generated electricity is then transmitted through undersea cables to an offshore substation, which consolidates the power from multiple turbines.

The offshore substation acts as a pivotal connection point, collecting and elevating the voltage of the electricity before transmitting it via subsea cables to an onshore substation, as shown in Figure 2.2. At the onshore substation, the voltage is further increased, enabling the seamless integration of the electricity

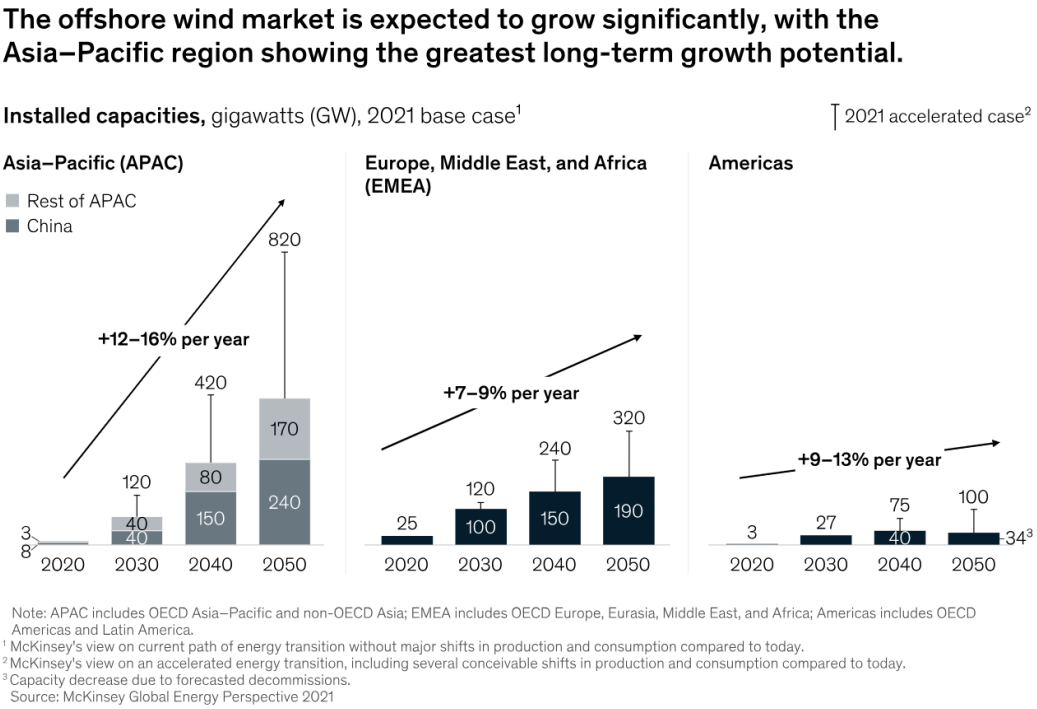

Figure 2.1: Offshore wind market installed capacities [10]

into the wider power grid. This grid-connected electricity is then distributed for consumption by homes, businesses, and industries.

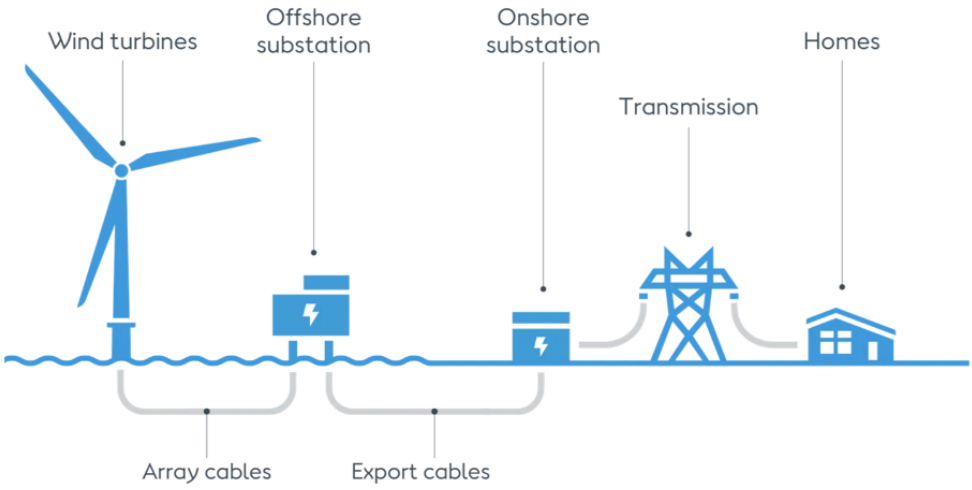

Figure 2.2: Power transmission from offshore to onshore [11]

To anchor the turbines securely to the seabed, various support structures like monopiles, jackets, or floating platforms are employed. These structures not only provide stability but also facilitate the efficient functioning of the turbine components. Emphasizing performance optimization, offshore wind farms incorporate monitoring and control systems that enable real-time data analysis. These systems aid in the identification of potential issues, allowing for proactive maintenance measures and minimizing operational downtime.

Beyond the technical aspects, offshore wind power offers distinct advantages. The offshore environment provides higher and more consistent wind speeds compared to onshore locations, especially related to wind energy potential [12]. Additionally, situating turbines at sea mitigates visual and noise impact on coastal communities, while the expanses of open water offer substantial space for large-scale wind farm development, where larger wind turbines can be installed [13]. Furthermore, another positive aspect is its proximity to densely populated coastal areas that reduce transmission losses, thereby enhancing overall energy efficiency.

It is also important to mention that offshore wind is a growing sector of the wind energy market with unique characteristics that enable large, utility-scale electric-generating facilities to be built adjacent to populated load centers, with manageable interactions with the environment and other ocean use activities. These projects can access more energy from ocean winds than adjacent projects on land, avoid high real estate costs and numerous siting conflicts in populated areas [12]. In essence, offshore wind power represents a critical component in the global transition to sustainable and renewable energy sources, meeting the escalating demand for clean electricity while prioritizing environmental considerations.

As a result, in 2022, the global offshore wind energy sector experienced its second-highest year of growth, with the commissioning of 8,385 MW in new projects. This substantial increase brought the total global capacity to 59,009 MW, spread across 292 operational projects, featuring over 11,900 wind turbines. Notably, for the consecutive second year, China spearheaded the global surge by commissioning an impressive 5,719.6 MW. The United Kingdom followed with the next significant annual deployment of 1,386 MW, trailed by France (480 MW), Germany (342 MW), Vietnam (331 MW), and the rest of the world contributing 126.5 MW, as reported by the National Renewable Energy Laboratory Offshore Wind Database in 2021.

In the midst of the global effort to shift towards sustainable energy, offshore wind power plants have gained considerable attention as a promising solution with a thriving global market. Recognizing their advantages and potential, there is an increasing acknowledgment of the importance of integrating these plants into various energy systems. In the specific context of the Brazilian energy scenario, exploring offshore wind power presents exciting possibilities for generating clean energy, with great complementary with hydroelectric power, predominant in the Brazilian energy matrix [14]. Nevertheless, an important aspect to be considered

and studied is the environmental licensing environment in Brazil, that is still on its early stages.

2.2 Environmental licensing in Brazil

The environmental licensing framework for offshore wind power involves a structured process aimed at assessing and mitigating potential environmental impacts associated with the development, construction, and operation of offshore wind projects. This process is essential for ensuring the sustainable deployment of offshore wind power while adhering to environmental regulations and minimizing negative ecological effects. It is traditionally composed by the Preliminary Environmental Impact Assessment (EIA), the comprehensive environmental impact assessment upon selecting a suitable site, permitting and authorization, monitoring and compliance and decommissioning considerations. Nonetheless, the environmental licensing process for offshore wind power projects exhibits variations among different countries, reflecting diverse regulatory frameworks, environmental priorities, and stakeholder engagement approaches.

Denmark, for example, employs a well-established licensing process governed by the Danish Energy Agency. The process includes a detailed EIA and requires developers to engage with relevant authorities, municipalities, and the public. Licensing considerations incorporate environmental protection, and adherence to the Danish Forest and Nature Agency guidelines is essential. In the UK, the environmental licensing process is regulated by the Planning Act 2008, ensuring that offshore wind projects undergo a rigorous Environmental Impact Assessment (EIA) to evaluate potential environmental impacts. Additionally, the Marine Management Organization oversees licensing, and successful projects receive development consent. As another example, Germany follows a stringent environmental licensing framework governed by the Federal Immission Control Act, in a process that involves a comprehensive EIA, where public participation is encouraged. The Federal Maritime and Hydrographic Agency, along with regional authorities, manages the licensing process. Projects must align with the Federal Requirements for Offshore Wind Energy, ensuring compliance with environmental standards [15].

In order to regulate the construction and operation of offshore wind power plants in Brazil, the federal body responsible for the administration of natural resources in Brazil, IBAMA (Instituto Brasileiro do Meio Ambiente e dos Recursos Naturais Renováveis), determined a specific process for its environmental licensing considering a technical and legal perspective. The document containing the instructions and environmental requirements for projects approval associated with construction and operation requests is a recent outcome of a partnership established in 2019 between IBAMA and the European Union through the program sector dialogues,

that focus on the exchange of experiences and the collection of elements to support the Brazilian government in the formulation and implementation of policies related to energy efficiency also covering the scope of environmental policy.

On July 2019, the International Workshop on Environmental Impact Assessment in Offshore Wind Complexes was held in order to facilitate knowledge exchange between European specialists in the field (Germany, Belgium, Norway, Portugal and United Kingdom) and several Brazilian institutions such as Aneel (Agência Nacional de Energia Elétrica), EPE (Empresa de Pesquisa Energética), CIRM (Comissão Interministerial para os Recursos do Mar), Cemave (Centro Nacional de Pesquisa e Conservação de Aves Silvestres), UFRN (Universidade Federal do Rio Grande do Norte) and UFRJ (Universidade Federal do Rio de Janeiro). As a further result of the workshop, an article associated to UFRN was published, presenting the current environmental planning and licensing models adopted by Germany, Belgium, Denmark, Spain, France and Portugal. Based on the study cases, on November 2020, the Standard Terms of Reference (TR) for Environmental Impact Assessment and Environmental Impact Report (EIA/Rima) for Offshore Wind Complexes was published, with the following name in Portuguese: Termo de Referência (TR) Padrão para Estudo de Impacto Ambiental e Relatório de Impacto Ambiental (EIA/Rima) de Complexos Eólicos Marítimos.

2.2.1 Standard Terms of Reference for Environmental Impact Assessment

The TR aims to determine the general technical guidelines, requirements and criteria that should underpin the EIA and Rima, in order to subsidize the prior environmental licensing process of IBAMA. It aims to cover projects including wind power generating units, the subsea substation, the energy transmission network, including its submarine section and its underground terrestrial section, as well as the aerial segment up to the connection with the National Interconnected System (SIN), System (SIN), the onshore substation and the support areas exclusively for the worksite. It is composed by 15 main sections: introduction, identification, characterization of the project/activity and its alternatives, technological and locational alternatives, area of study, diagnosis, government bodies involved, environmental impact analysis, area of environmental influence, environmental risk analysis, environmental management plan, conclusion, references, glossary, and environmental impact report. For the scope of this work, a further analysis will be held involving area of study, diagnosis, environmental impact analysis, environmental risk analysis, environmental management plan and environmental impact report.

Area of study

The Study Area covers the territory in which there is continuity of environmental, physical, biological and socio-economic factors that are considered relevant to understanding the impacts and for the future definition of the project's Area of Influence. The territorial choice must be duly justified, including which environmental factors were analyzed, the area covered by these factors and the degree of significance attributed to them. Furthermore, these studies must provide information for environmental diagnosis, the choice of locational and technological alternative and for the technical basis of the prognosis that will or will not attest to the socio-environmental viability of the project.

Diagnosis

Sequentially, this section presents the environmental diagnosis of the selected area of study. The diagnosis development includes the description and utilization of a scientifically proven and compatible methodology, based on the gathering, organization, consolidation and analysis of primary data. As a result, the diagnosis aims to comprise a full description and analysis of environmental resources and its interactions, in order to characterize the environmental situation of the locality before the project implementation.

The following categories of data have the potential to be collected by satellites, and will be further evaluated in the next chapter.

- climatology and meteorology
- oceanography
- noises and vibrations
- geology, geomorphology, pedology and geotechnics
- water quality and hydrodynamics
- territorial and landscape dynamics

Environmental impact analysis

Based on the gathered data provided by the diagnosis phase, the environmental impact analysis aims to identify, describe and systematically evaluate the environmental impacts generated during the planning, installation, operation (normal and abnormal associated with operational deviations, incidents, accidents, etc.) and decommissioning of the project or activity, considering the entire project, in

the terrestrial and marine environments. Throughout the analysis, all methods, techniques and criteria must be properly identified.

In order to fulfill its goal, this section analyzes the environmental impacts of the project and its alternatives, by identifying, predicting the magnitude and interpreting the importance of the likely relevant impacts, discriminating between: positive and negative impacts (beneficial and adverse), direct and indirect, immediate, medium and long term, temporary and permanent; their degree of reversibility; their cumulative and synergistic properties; the distribution of social burdens and benefits. Moreover, it comprises the identification of levels of uncertainty regarding impacts, based on the availability and quality of data from theand international experience on the confirmed impacts of offshore wind typology, as well as compensatory measures for remaining negative impacts.

In addition, it must present tables for the different stages (planning, installation, operation and decommissioning), which includes the generating activities, the environmental aspects and the environmental factors affected, a summary description of each environmental impact and the preventive, mitigating or compensatory measure, and also maximum acceptable occurrence parameters for each negative impact. Lastly, the Environmental Compensation Plan must be presented, as determined by Ibama Normative Instruction 08/11.

Environmental risk analysis

The environmental risk analysis intends to identify the main risks of the the environment and the external community, during both installation and operation phases, following two mains steps:

1. Present the location of the development and its units on a map with adequate resolution and scale.

2. Provide a succinct and objective description of the area of influence, using whenever possible maps, highlighting: (i) meteoceanographic data, (ii) water bodies, (iii) populated areas in the vicinity of the project, (iv) environmentally sensitive or protected areas, (v) activities in the vicinity of the project. (iv) environmentally sensitive or protected areas, (v) economic and/or extractive activities, among others, which may be affected in the event of an accident involving the project accident.

3. Describe any other activities carried out during the installation of the project that may present risks to the environment or the external community.

4. Classify each hazard within categories of frequency and severity

5. Present a spreadsheet containing the hazards identified, their classification in terms of frequency, consequence and level of risk, as well as preventive and/or mitigating actions, which should be detailed in the Risk Management Program.

6. Present a conclusion considering the tolerability of the risks detected in relation to the socio-environmental sensitivity of the project area.

Based on the risks identified, a proposal for the Risk Management Program (RMP) must be presented, including the installation and operation phase of the project. The RMP should contain, for each phase, a description of the activities involving the risks identified (e.g. procedures for refueling machinery), preventive measures to avoid an accident (e.g. measures to prevent fuel from leaking during refueling) and the Emergency Plan, with a response structure to deal with the accident scenarios identified. If the project is feasible, the RMP should be detailed at a later stage

Environmental management plan

Succeeding the environmental risk analysis, the environmental management plan presents, in a conceptual way, the plans, programs and measures to be adopted in all phases of the project to avoid, mitigate or compensate for adverse impacts and enhance beneficial impacts, indicating the factors and parameters to be considered. Furthermore, it proposes follow-ups and monitoring programs (positive and negative impacts), which use predefined indicators, with the aim of verifying the effectiveness of the measures and the occurrence of the impact, as well as establishing the actions to be taken.

Environmental impact report

As a consolidation of all the analyses carried out during the elaboration of the Environmental Impact Study, the environmental impact report (RIMA) is a summary of the environmental impact assessment, which presents the analysis of the environmental, social and economic conditions in the project/enterprise area in an objective and appropriate manner. For its development and execution, the guidelines are contained in Article 9 of Conama Resolution 01/1986.

Chapter 3

Data collection

In Earth Observation, the availability of open source satellite data has become a cornerstone for diverse applications, offering an extensive and freely accessible repository of information. When it comes to open source satellite data providers, there are projects and organizations that stand out, specifically Aeolus, NOAA (National Oceanic and Atmospheric Administration), and EUMETSAT (European Organization for the Exploitation of Meteorological Satellites), with great significance within the engineering domain.

The National Oceanic and Atmospheric Administration (NOAA), linked to the US government, plays an important role in providing open access to a multitude of satellite data. NOAA's satellite constellation, including polar-orbiting and geostationary satellites, captures crucial information for weather prediction, climate monitoring, and environmental research. The Advanced Weather Interactive Processing System (AWIPS) and the Comprehensive Large Array-Data Stewardship System (CLASS) serve as gateways for accessing NOAA's satellite data. Using NOAA's datasets, it is possible to enhance weather modeling, study climate patterns, and bolster disaster preparedness and response strategies.

On the other hand, EUMETSAT is the European operational satellite agency for monitoring weather, climate and the environment from space, a collaborative organization comprising 30 European countries, that specializes in the exploitation of meteorological satellites. It operates a fleet of satellites, including those in the Meteosat and Metop series, offering a comprehensive suite of observations for weather forecasting, climate monitoring, and environmental analysis. The agency's commitment to open data access aligns with the principles of Copernicus, fostering a collaborative ecosystem where engineers that facilitates efficient retrieval of information for research and application development in the engineering domain.

Copernicus, the European Union's Earth Observation Program, stands as a leading contributor to open source satellite data. Operated by the European Space Agency (ESA) and the European Organisation for the Exploitation of

Meteorological Satellites (EUMETSAT), Copernicus provides a wealth of data encompassing atmospheric composition, ocean dynamics, land cover, and climate change indicators. The Sentinel satellite series, a fundamental component of Copernicus, delivers high-resolution imagery and radar data, empowering the control of environmental changes, assess land use, and response to natural disasters with unprecedented accuracy.

Lastly, the European Space Agency's (ESA) Aeolus project represents a pioneering initiative in Earth observation and data collection, dedicated to wind measurements. Launched on August 22, 2018, the Aeolus satellite is equipped with the Atmospheric Laser Doppler Instrument (Aladin), utilizing advanced laser technology to measure global wind profiles from space. The primary goal of the Aeolus mission is to provide observations of global wind profiles along the instrument line of sight direction over a minimum lifetime of three years, demonstrating the Doppler Wind Lidar technique for measuring wind profiles from space.

In order to conduct a feasibility study on the usage of satellite data for the construction and operation of offshore wind power plants, it is wise to first divide the data to be collected into two different categories depending on the stage of progress of the offshore wind power plant project. First, there is data associated with the licensing and environmental impact study, then the data related to the construction, operation, control and maintenance of the site, focusing mainly on wind parameters.

3.1 Licensing and environmental impact study

As mentioned in section 2.1.1 of Chapter 1, the licensing process in Brazil involves the following groups of data:

- climatology and meteorology
- oceanography
- noises and vibrations
- geology, geomorphology, pedology and geotechnics
- hydrodynamics and water quality
- territorial and landscape dynamics

3.1.1 Climatology and meteorology

Climatology and meteorology are distinct yet closely related branches of atmospheric sciences. Meteorology focuses mainly on short-term atmospheric conditions, including phenomena such as temperature, humidity, precipitation, and wind patterns

over relatively short time spans, typically hours to days. Alternatively, climatology examines long-term weather patterns and statistical trends over extended periods, often spanning decades to centuries. While meteorology is concerned with the immediate state of the atmosphere, climatology seeks to understand the broader climatic trends and variations. In the context of environmental impact analysis for offshore wind power plants, climatology and meteorology play crucial roles in assessing the potential effects on the surrounding environment.

Meteorological data, including wind speed and direction, are essential for assessing the wind resource at offshore locations. Long-term wind climate data derived from climatological studies helps understanding the seasonal and inter-annual variations, providing valuable insights for optimal turbine siting and design, as all enabling better anticipation of variations in wind patterns, optimizing maintenance schedules, and ensuring the longevity and efficiency of the offshore wind power plant. Siemens Gamesa SG 11.0-200 DD turbine, for example, is known for its large rotor diameter and high capacity factor, making it suitable for high-wind offshore environments [16]. Moreover, both meteorology and climatology contribute to the evaluation of extreme weather events, such as storms and hurricanes, as their occurrence and potential future changes in extreme weather patterns is vital for designing offshore wind structures capable of withstanding these events.

Additionally, climate data is also used to study migratory patterns of birds and marine life, considering factors such as wind corridors and seasonal variations. This information aids in predicting and mitigating potential impacts on local ecosystems, informing the environmental impact assessment. Besides, climatology contributes to assessing the potential impacts of climate change on offshore wind projects. This involves studying long-term climate trends and variations to anticipate shifts in wind patterns, sea level rise, and other climatic factors that may influence the project's resilience and longevity.

In order to access meteorology and climatology data over-viewing Brazil, key resources are INPE, CBERS, AQUA and Terra Satellites, GOES and Metop Satellites from EUMETSAT. INPE (National Institute for Space Research) is Brazil's leading space research institution, operating various satellite missions, including the Amazonia-1 satellite, which can offer insights into land cover, vegetation, and climate patterns in Brazil. The CBERS program (China-Brazil Earth Resources Satellite Program), provides high-resolution EO data, specially when it comes to monitoring land use, vegetation, and environmental changes in Brazil. NASA's AQUA and Terra satellites contain instruments such as MODIS (Moderate Resolution Imaging Spectroradiometer), offering observations on atmospheric conditions, land surface temperatures and cloud cover over Brazil. In addition, NOAA's GOES (Geostationary Operational Environmental Satellites) provide continuous monitoring of weather conditions in the Americas, specially GOES-East and GOES-West, the ones that offer real-time and historical data on parameters such as cloud cover

and atmospheric moisture. Lastly, Metop Satellites from EUMETSAT contribute to global atmospheric monitoring, even though EUMETSAT's primary focus is on Europe. Instruments like the Advanced Scatterometer (ASCAT) on Metop satellites supply wind data that can be relevant for meteorological studies in Brazil.

3.1.2 Oceanography

Oceanography is the scientific field concerning all aspects of the world's oceans and seas, including their physical and chemical properties, their origin and geologic framework, and the life forms that inhabit the marine environment. When it comes to ocean-related data for Brazil, the most relevant sources are NASA's OB.DAAC and EOSDIS, JAXA's GCOM-W1 Satellite, CMEMS, Sentinel-3 Satellites from Copernicus, NOAA's National Centers for Environmental Information (NCEI) and ESA's Climate Change Initiative (CCI) Sea Level Project.

The Earth Observing System Data and Information System (EOSDIS) provides datasets such Sea Surface Temperature (SST) from instruments like MODIS on AQUA and Terra satellites, and ocean color data from sensors such as OLCI (Ocean and Land Color Instrument) on the Sentinel-3 satellite, offering insights into sea surface conditions. On the other hand, Ocean Biology Distributed Active Archive Center (OB.DAAC) is a NASA data center specializing in ocean biology data sets, enabling access to ocean color data, chlorophyll concentrations, and other bio-optical properties measured by instruments like MODIS. The Global Change Observation Mission - Water (GCOM-W1) satellite, operated by the Japan Aerospace Exploration Agency (JAXA) produces data on sea surface temperature, contributing to ocean-related studies. Sentinel-3, part of the Copernicus program, is specifically designed for ocean monitoring, responsible for producing data on sea surface temperature, ocean color, and sea surface height. NOAA's NCEI provides access to various ocean-related datasets, including sea surface temperature, ocean currents, and bathymetric data. NOAA's geostationary and polar-orbiting satellites contribute to monitoring ocean conditions. Lastly, the CCI Sea Level Project, a program of the European Space Agency (ESA), offers sea level data derived from satellite altimetry.

3.1.3 Noises and vibration

Noises and vibrations study concerns the assessment of underwater noise generated during construction and operation as well as the impact of noise and vibration on marine life, including marine mammals and fish. Accessing specific open-source satellite data related to ocean noise and vibration might be challenging, as traditional satellite sensors are not designed for capturing such parameters directly. However, indirect data related to oceanography and meteorology from sources

like EUMETSAT, NOAA, and Copernicus can be valuable for understanding environmental conditions that may contribute to noise and vibration. High winds and turbulent sea conditions can contribute to increased noise and vibration levels. In that sense, Copernicus' CMEMS provides information on ocean currents and wave height, while NOAA offers various marine and atmospheric datasets. It is important to highlight that ground-based measurements provide precise information about noise levels in the ocean, evidencing the value of deploying local sensors or hydrophones in the study area.

3.1.4 Geology, geomorphology, pedology and geotechnics

Geology is the scientific study of the Earth's structure, composition, and processes that have shaped its features over time. In the context of offshore wind power plants licensing and operation, geology plays a crucial role in assessing the seabed and subsoil conditions at the project site. Understanding the geological composition helps engineers evaluate the stability of the seabed, identify potential hazards such as fault lines or subsurface structures, leading to more informed decisions regarding the foundation design of offshore wind turbines. Similarly, geomorphology studies landforms, their origins, evolution, and the processes that shape the Earth's surface. It allows a further analysis on the underwater topography, submarine canyons, and the general shape of the sea, enabling the identification of potential areas of erosion or sedimentation, and understanding of the dynamics of the underwater landscape.

Pedology, on the other hand, is the study of soil, specifically focusing on its formation, classification, and distribution. As a consequence, pedological assessments can inform decisions related to soil compaction, load-bearing capacity, and the potential for sediment erosion or deposition over time. Ultimately, geotechnics, or geotechnical engineering, is the branch of civil engineering that deals with the behavior of Earth materials, critical for designing foundations that can withstand the dynamic forces of wind, waves, and currents. Geotechnical studies involve site investigations, soil sampling, laboratory testing, and analysis to determine the optimal foundation type and to ensure the long-term stability of the entire offshore structure.

One of the most relevant open-source satellite data source for geological and geomorphological studies is the Landsat Program from USGS and NASA, that provides high-resolution imagery that allows for land cover classification, identification of geological features and monitoring changes over time. Sentinel-1 and Sentinel-2 satellites from the Copernicus program provide radar and optical imagery, respectively. Sentinel-1's radar data is valuable for studying terrain deformation, subsidence, and ground stability, which are crucial for geotechnical assessments. Sentinel-2 offers high-resolution optical imagery for land cover classification and geomorphological analysis.

Moreover, NASA's Advanced Spaceborne Thermal Emission and Reflection Radiometer (ASTER) sensor on the Terra satellite provides data suitable for geological and land surface studies. ASTER's multispectral imagery aids in mapping geological formations and identifying surface materials. Another NASA program, the Shuttle Radar Topography Mission (SRTM) offers high-resolution digital elevation models (DEMs) that are valuable for studying terrain morphology, identifying geological structures, and assessing landforms relevant to geotechnics. Additionally, commercial satellites like WorldView-2 and WorldView-3 from Maxar Technologies provide high-resolution optical imagery, allowing detailed mapping of land cover, geological features, and terrain characteristics.

3.1.5 Hydrodynamic and water quality

Hydrodynamic considerations dictates the assessment of wave and current loads, scouring, sediment transport, and dynamic response analyses. As these factors directly influence the structural integrity of turbines and support structures in offshore wind power plants, comprehensive evaluations during the licensing phase to ensure design resilience against extreme conditions are needed. Water quality considerations are equally vital, involving the complex interplay of factors such as sediment resuspension, chemical runoff, and biofouling. Construction and maintenance activities can lead to sediment resuspension, affecting water clarity and potentially impacting marine ecosystems.

Similarly to the sources indicated on the oceanography session, CMEMS and Sentinel Satellites play an important role, providing data associated with sea surface temperature, sea level, and ocean currents. In parallel, Visible Infrared Imaging Radiometer Suite (VIIRS) on NOAA/NASA satellites offers data on ocean color, sea surface temperature, and atmospheric parameters. Furthermore, another tool to be applied is the Hybrid Coordinate Ocean Model (HYCOM), that offers information on ocean currents and temperature, aiding in the analysis of hydrodynamic conditions.

3.1.6 Territorial and landscape dynamics

Territorial and landscape dynamics refer to the continuous changes and transformations in the physical, environmental, and spatial characteristics of a given territory or landscape. This includes alterations in land use, vegetation patterns, coastline configurations, and overall environmental features over time. Territorial and landscape dynamics influence the initial site selection for offshore wind power plants as changes in coastal morphology, seabed topography, and environmental conditions may impact the suitability of a site.

As seen before, Sentinel-1 and Sentinel-2 satellites from Copernicus offer radar

and optical imagery, respectively, providing insights on territorial and landscape dynamics through changes in coastal morphology, land use, and vegetation cover. NASA's Landsat also plays a major due to providing imagery with long historical record, enabling land cover, vegetation and urban development analysis over time. Moreover, VIIRS provides data on nighttime lights, which can be indicative of urban development and changes in human activity. Another key source is INPE, that operates satellites such as CBERS (China-Brazil Earth Resources Satellite) and Amazonia-1, which provide data specific to Brazil. Collaborating with INPE can offer access to regional datasets relevant to territorial and landscape dynamics in Brazil.

At the same time, commercial satellites like WorldView-2 and WorldView-3 offer high-resolution optical imagery, enabling detailed analysis of landscape features, urban development, and changes in land cover. In addition, the Global Urban Footprint dataset, produced by the German Aerospace Center (DLR), provides high-resolution global maps of human settlements, useful for studying urban expansion and changes in land use, contributing to assessments of landscape dynamics. Lastly, Google Maps can also be a powerful tool, as it is platform to access and analyze a variety of satellite datasets, including Landsat, Sentinel, and MODIS.

3.2 Wind monitoring

In order to develop a feasibility study on the construction and operation of offshore wind farms, the most important parameters are associated with wind properties. A comprehensive approach to monitoring wind properties involves the integration of on-site and satellite-based tools, such as anemometry towers, LIDAR systems, SODAR systems, met masts, and remote sensing devices, all designed to provide direct measurements of wind speed, direction, and atmospheric conditions at the project site.

Anemometry towers equipped with various sensors offer crucial data on wind profiles at different heights. Lidar systems contribute to detailed vertical profiles of wind conditions using laser beams. Sodar systems use sound waves to measure wind profiles, offering insights into atmospheric conditions and turbulence. Meteorological masts, or met masts, with an array of sensors, provide meteorological data essential for wind resource assessments. Additionally, portable remote sensing devices like WindCube and ZephIR Lidar facilitate short-term wind measurements at different locations within the project site.

Satellite-based tools further enhance wind monitoring capabilities, such as Sentinel-1 and Sentinel-2 from Copernicus, that offer radar and optical imagery, respectively. Sentinel-1 provides interferometric synthetic aperture radar (InSAR) data for monitoring ground movement, while Sentinel-2 aids in understanding land

cover changes influencing wind patterns. WindSat, ASCAT, QuikSCAT, and RapidScat satellites provide global wind speed and direction measurements, especially over the ocean, contributing valuable information for offshore wind conditions. Additionally, The ERA5 reanalysis data from the European Centre for Medium-Range Weather Forecasts (ECMWF) is a global atmospheric dataset offering historical records of wind speed and direction at various altitudes, facilitating long-term trend analysis.

As discussed earlier on this chapter, EUMETSAT provides access to a range of satellite observations, including those related to wind parameters. Satellite instruments such as ASCAT (Advanced Scatterometer) on EUMETSAT satellites provide accurate measurements of wind speed and direction over the ocean. These data sets, often available at high spatial and temporal resolutions, contribute to the understanding of the wind climate in the target region. Due to EUMETSAT's global coverage, it is possible to ensure that offshore wind sites in Brazil can be thoroughly assessed, essential for identifying specific areas with consistent and favorable wind conditions in order to maximize energy yield and turbine layout. Furthermore, its archives of historical data enable the analysis of long-term wind variability. Beyond wind parameters, EUMETSAT data can aid in assessing additional environmental factors such as sea surface temperature, atmospheric pressure, and wave height, integral to the holistic evaluation of the offshore site, considering both the technical and environmental aspects.

The Aeolus satellite mission, conducted by ESA, also emerges as an excellent choice for the collection and analysis of wind data, particularly wind speed. Launched in 2018, Aeolus is equipped with the Atmospheric Laser Doppler Instrument (Aladin), a state-of-the-art technology designed explicitly for measuring global wind profiles from space. This capability provides a unique opportunity for acquiring high-resolution and three-dimensional wind data, crucial for the feasibility study outlined in this master thesis. Moreover, the Aeolus VirES (Virtual Erath Explorer Server) complements this initiative by providing an efficient, web-based and user-friendly platform for accessing and analyzing the Aeolus wind data, allowing comprehensive insights into wind behaviour in the target region.

Chapter 4

Site selection for offshore wind farms

Beyond the environmental and socioeconomic spheres, the selection of an appropriate site for offshore wind farms comprises a complex and critical technical analysis of wind parameters in order to ensure the success and viability of wind energy projects. Understanding and characterizing wind patterns at potential sites is paramount to optimizing energy yield, mitigating operational risks, and ensuring the long-term sustainability of offshore wind power plants.

In that sense, wind behavior analysis involves the study of wind patterns, including wind speed, direction, and turbulence. It is influenced by a range of factors such as topography, atmospheric conditions, and oceanic interactions. As a result, a comprehensive analysis of different wind parameters is crucial to ensure a holistic understanding of the wind resource at potential sites.

4.1 Wind parameters for site selection

4.1.1 Wind Speed (v)

As expected, wind speed is one of the most important parameters directly impacting the energy yield of wind turbines, given by the amount of electrical energy produced by the turbine over a given period of time. In that sense, wind turbines are designed with a power curve, showed in Figure 4.1 that illustrates the relationship between wind speed and power output, modelled as follows [17]:

$$P(v) = P_r \begin{cases} 0 & v < v_c \\ \frac{v^3 - v_c^3}{v_r^3 - v_c^3} & v_c \leq v \leq v_r \\ 1 & v_r \leq v \leq v_f \\ 0 & v \geq v_f \end{cases} \tag{4.1}$$

where v_c, v_r and v_f are, respectively, the cut-in, rated and cut-out wind speeds. The first parameter, the cut-in speed, is the minimum wind speed at which a wind turbine starts generating power. The rated speed, on the other hand, indicates the wind speed at which the turbine operates most efficiently, generating its maximum rated power. Alternatively, cut-out speed is the maximum speed at which the turbine automatically shuts down in order to prevent damage and protect the turbine from excessive forces during high wind conditions. In general, the cut-in speed (v_c) typically ranges from 3 to 4 m/s since, at lower wind speeds, there is insufficient torque applied to the blades, hindering their rotation, while the cut-out speed (v_f) is typically set at 25 m/s to prevent damages, and the rated speed (v_r) varies between 11 and 17 m/s, influenced by local wind conditions. Figure 4.2, for instance, illustrates the power curve using actual data for a group of wind turbines at a wind farm.

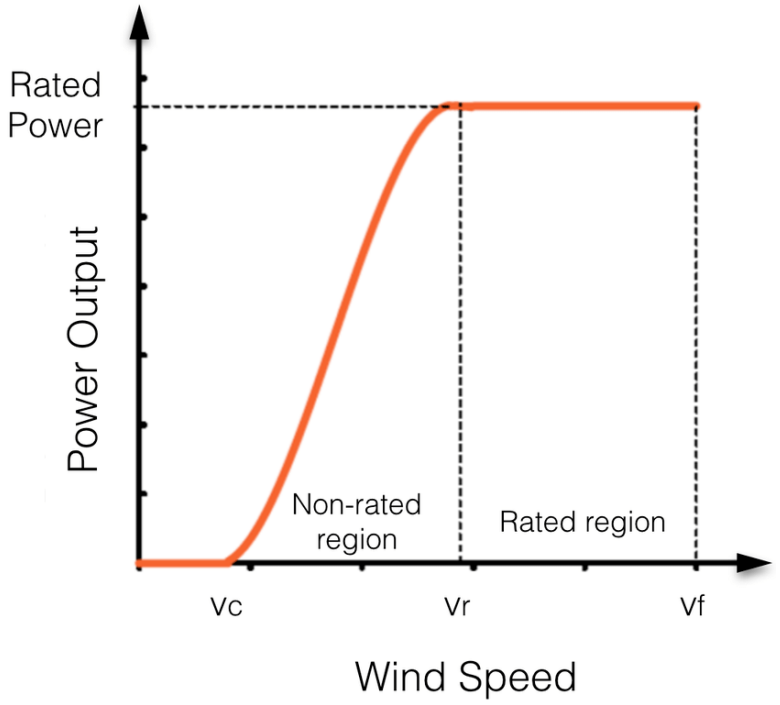

Figure 4.1: Wind turbine power curve [17]

Considering the air density ρ, and A the swept area of the turbine rotor, the

power from the wind (P) by a turbine is determined by the equation:

$$P \propto \frac{1}{2}\rho A v^3 \tag{4.2}$$

The kinetic energy available for power generation is then directly proportional to the cube of the wind speed. That way, analyzing wind speed data, obtained through anemometry or remote sensing technologies, is crucial for assessing the energy potential of a given site. For instance, on a study conducted in Northeast Brazil, increases in wind speed led to 50-57% increases in electricity generated at new wind power plants in Northeast Brazil [18].

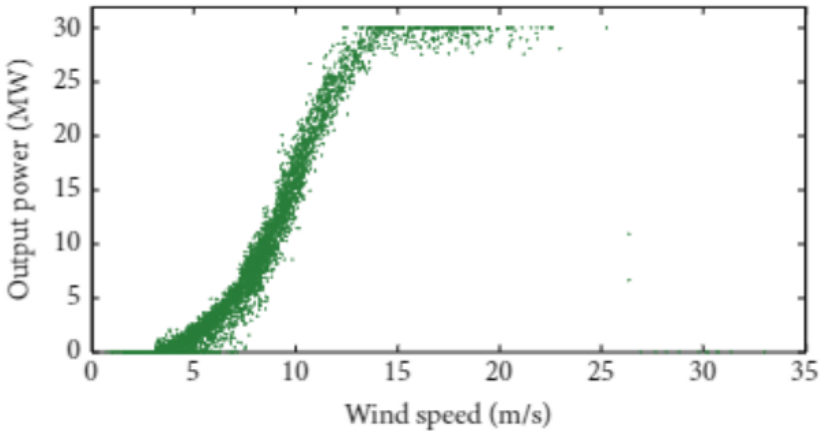

Figure 4.2: Power curve using actual data for a group of wind turbines at a wind farm [19]

An important parameter for energy production is the Betz limit, proposed by German physicist Albert Betz in 1919, that represents the theoretical maximum efficiency achievable by a wind turbine. Betz determined this limit to be 59.3% ($C_{p,max} = 16/27$), meaning that, in principle, only up to 59.3% of the kinetic energy from the wind can be harnessed to rotate the turbine and produce electricity. In practice, actual turbines fall short of reaching the Betz limit, and typical efficiencies for modern wind turbines generally range between 45% and 50%. Generally, the power coefficient (C_p), a dimensionless factor that represents the efficiency of a wind turbine in converting the kinetic energy of the wind into electrical power, is expressed as:

$$C_p = \frac{P}{\frac{1}{2}\rho A v^3} \tag{4.3}$$

Another form of defining the performance coefficient C_p is in terms of the rotor diameter, shown in equation 4.4:

$$C_p = \frac{P}{\frac{1}{2}\rho(\frac{\pi D^2}{4})v^3} \tag{4.4}$$

Additionally, it is interesting to punctuate that the power coefficient (C_P) is a measure of the proportionality expressed in equation 4.2. That way, analyzing wind speed data allows the determination of available kinetic energy and the assessment of energy conversion efficiency.

4.1.2 Wind direction θ

Wind direction significantly influences turbine layout optimization to maximize energy capture, specially due to an effect called the "wake effect". Wind turbines operate by extracting energy from the wind to generate electricity, resulting in the downstream wind having lower energy content and reduced speed, forming what is known as the wake of the turbine. As this wake progresses downstream, it gradually dissipates and returns to free stream conditions. If the wake intersects with the swept area of a downwind turbine, the downwind turbine becomes shadowed by the turbine generating the wake, as can be seen in Figure 4.3 and Figure 4.4.

The consequences of a wake include a decrease in wind speed, subsequently reducing the overall energy production of the wind farm, and an elevation in wind turbulence, potentially leading to heightened dynamic mechanical loading on downwind turbines. These effects underscore the importance of considering and managing wakes during the design and operational phases of wind farms, as it holds significance not only for individual generators but also for the overall performance of the wind farm.

The Biot-Savart law, employed to model wake effects, is expressed by:

$$v = \frac{1}{4\pi}\frac{\Gamma}{r} \tag{4.5}$$

where v is the induced velocity, Γ is the circulation of the rotor and r is the radial distance from the rotor center.

Wake effects are also influenced by the Jensen wake model, predicting the wind speed deficit in a turbine's wake in terms of the wind speed deficit Δv, the axial induction factor a, the undisturbed wind speed U_0, the wake expansion parameter k, the downstream distance from the turbine x and the rotor diameter D, as seen in the equation below. In general, the wake effect has the default value $k = 0.075$ for most land-cases, while for offshore applications it is recommended to use a lower limit of $k = 0.04$ [21].

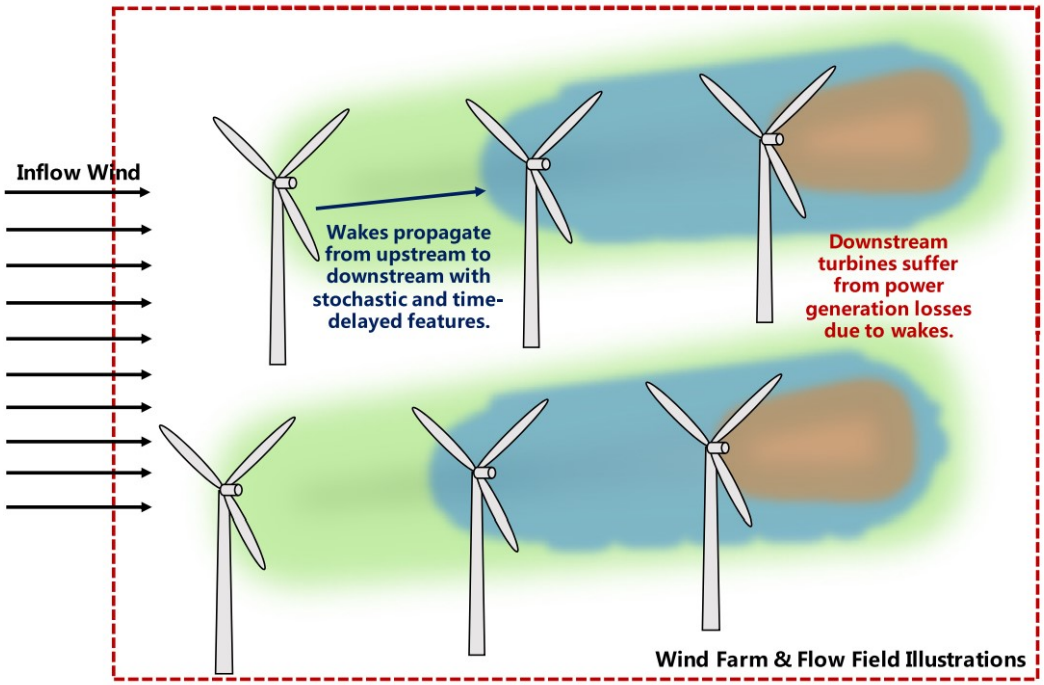

Figure 4.3: Illustration of wake effects on a wind farm [20]

$$\Delta v = \frac{2 \cdot a}{1 + 2 \cdot a} \cdot \frac{U_0}{\left(1 + \frac{2 \cdot k \cdot x}{D}\right)^{1/2}} \tag{4.6}$$

In order to enable the wind turbines to align with the wind direction, they are equipped with yaw control systems, that use feedback from wind direction sensors to adjust the yaw angle of the turbine. When a misalignment occurs and the turbine faces a different direction than the incoming wind, the efficiency is reduced and there are increasing loads on the turbine structure.

4.1.3 Load analysis

Load analysis involves examining dynamic loads on turbine components. One way of modelling aerodynamic loads is through the Blade Element Momentum (BEM) theory, a model that combines the blade element and momentum theories, the blade element being the theory that allows for the computation of the loads acting on a rotor based on the geometric and aerodynamic properties of individual spanwise blade sections. BEM is the mainstay of wind turbine industry for predicting wind turbine performance, and can be roughly reduced to the following equation:

Figure 4.4: Wake interactions in Horns Rev Offshore Wind Farm, Denmark. Photo by Christian Steiness / Vattenfall

$$F = \frac{1}{2}\rho v^2 A C_l \tag{4.7}$$

The equation above considers F as the aerodynamic force and C_I the lift coefficient.

4.1.4 Turbulance Intensity (TI)

Turbulence is a flow regime distinguished by variations in pressure and velocity, the separation of boundary layers, the formation of vortex structures, and disturbances in the fluid flow. In such wise, turbulence intensity characterizes wind speed variability, critical for structural loads and performance analysis. The von Kármán spectral model relates turbulence intensity (TI) to the standard deviation of wind speed (σ) and the mean wind speed (v):

$$TI = \frac{\sigma}{v} \tag{4.8}$$

As a result, the power coefficient C_p, defined in 4.3, is also affected by turbulance intensity, leading C_p to lower values when turbulence is high. In that case, there is a reduction in energy conversion.

Considering $C_p(TI)$ the power coefficient adjusted for turbulence-effects, the power equation with turbulence intensity considerations can be expressed as:

$$P = \frac{1}{2}\rho A C_p(TI) v^3 \tag{4.9}$$

Turbulence affects also the aerodynamic loads on the turbine blades, as the turbulence in the wind causes fluctuations in wind speed, direction, and pressure, leading to dynamic changes in the aerodynamic forces acting on the turbine. This dynamic wind loading, resulting from turbulence, can subject wind turbine components to higher peak loads compared to steady, non-turbulent conditions, contributing to dynamic loads that may exceed the design limits of the turbine.

The International Electrotechnical Commission (IEC) provides standards for measuring and assessing turbulence intensity in the context of wind turbine performance. IEC defines that turbine classes are determined by three parameters: the average wind speed, extreme 50-year gust, and turbulence, as shown in Table 4.1

In brief, lower turbulence intensity indicates stable wind conditions, reducing dynamic loads on turbine components, therefore optimizing performance. Turbulence reduces wind direction, power coefficient, and power output, and can affect the wake effect downstream, affecting wind speed and performance of other turbines downwind [22].

4.1.5 Wind shear (dv/dz)

Wind shear, also known as wind gradient, is a meteorological occurrence characterized by a swift change in wind direction and/or speed over a specified distance, as illustrated by Figure 4.5 . This phenomenon can manifest at various flight levels, but it presents particular hazards at lower altitudes, extending up to around 2,000 feet in height, and affects wind power generation in several ways. Firstly, it leads

Wind Class/Turbulence	Annual Avg. Wind Speed	Extreme 50-Year Gust
Ia High - Higher Turbulence	10 m/s (36 km/h; 22 mph)	70 m/s (250 km/h; 160 mph)
Ib High - Lower Turbulence	10 m/s (36 km/h; 22 mph)	70 m/s (250 km/h; 160 mph)
IIa Medium - Higher Turbulence	8.5 m/s (31 km/h; 19 mph)	59.5 m/s (214 km/h; 133 mph)
IIb Medium - Lower Turbulence	8.5 m/s (31 km/h; 19 mph)	59.5 m/s (214 km/h; 133 mph)
IIIa Low - Higher Turbulence	7.5 m/s (27 km/h; 17 mph)	52.5 m/s (189 km/h; 117 mph)
IIIb Low - Lower Turbulence	7.5 m/s (27 km/h; 17 mph)	52.5 m/s (189 km/h; 117 mph)
IV	6.0 m/s (22 km/h; 13 mph)	42 m/s (150 km/h; 94 mph)

Table 4.1: IEC 61400: wind class and turbulence data

to non-uniform wind conditions across the height of the turbine rotor, influencing the distribution of aerodynamic forces on the turbine blades, and affecting the load analysis. Moreover, as seen previously on equations 4.2 and 4.3, the power equation for a wind turbine can be written as:

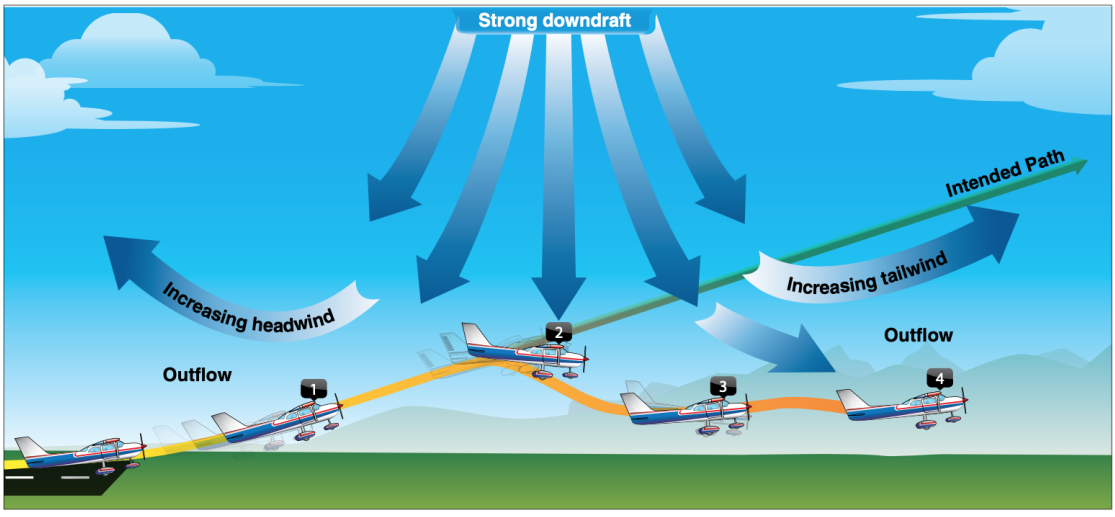

Figure 4.5: Wind shear illustration [23]

$$P = \frac{1}{2}\rho A C_p v^3 \tag{4.10}$$

To that equation, wind shear introduces a vertical gradient in wind speed $\frac{dV}{dz}$ that affects specially the power coefficient C_p, that becomes:

$$C_p(z) = C_p(0) \cdot \left(1 - k \cdot \frac{dV}{dz}\right) \tag{4.11}$$

where $C_p(0)$ is the power coefficient at the reference height, k is a coefficient related to the turbine and atmospheric conditions, and $\frac{dV}{dz}$ is the wind speed gradient.

Considering $v(z)$ the wind speed at height z, v_0 the reference wind speed at height z_0, and α the shear exponent, the power law equation describing wind shear is:

$$v(z) = v_0 \left(\frac{z}{z_0}\right)^{\alpha} \tag{4.12}$$

Wind shear also affects the fatigue loading on wind turbine components. The varying wind speed with height leads to cyclic loading on the blades and other structural elements, contributing to material fatigue over time. Wind shear can cause significant torque oscillations in wind turbines, affecting the back-electromotive force and electrical power of the generator [24]. Furthermore, unsteady horizontal wind shear induces a significant yaw moment on the rotor without affecting power generation, while extreme operational gust severely affects the turbine's performance parameters [25].

4.2 Study case from bibliography: wind speed trends and the potential of electricity generation at new wind power plants in northeast Brazil

As seen in this chapter, slight changes in wind speed can lead to generation variability at wind power plants. This article, despite the usage of a different data source for obtaining wind measurements, will be used as a guideline, providing a direction regarding the outputs to be found in the study case to be developed in the next chapter. The study was developed by Amanda Ribeiro de Andrade, Victor Felipe Moura Bezerra Melo, Daisy Beserra Lucena and Raphael Abrahão, and published by the Journal of the Brazilian Society of Mechanical Sciences

and Engineering, analyzing the wind speed trends and the potential of electricity generation at new wind power plants in the semiarid zone of Northeast Brazil [18].

Northeast, southeast and Southern regions of Brazil are considered to have the higher wind energy potential, mainly by the coast, where strong and steady winds are observed all year long. In this context, data from the 2017 Brazilian Wind Energy Atlas underscores that the dune regions along the Northeast coast of the state of Ceará exhibit an annual average wind speed of around 10 m/s [26]. While the research was conducted, there was an ongoing implantation process of a large scale onshore wind power plant complex. A minimum of 18 wind power facilities were in the planning stages, with three already operational. The combined installed capacity is projected to reach at least 565 MW. In that sense, the study aimed to explore potential trends in wind speed and assess their impact on wind electricity generation in the vicinity of the proposed sites for these new wind power plants.

Hourly wind speed data were obtained from two meteorological stations situated in the city of Patos (Latitude: 7°0′36″ S, Longitude: 37°15′36″ W) and in the São Gonçalo district within the city of Sousa (Latitude: 6°45′0″ S, Longitude: 38°12′36″ W). These data are accessible through the Brazilian National Institute of Meteorology (INMET) website, specifically through the Weather Data Base for Teaching and Research (BDMEP). Nevertheless, the collected data from the weather stations required adjustments to align with the height of the wind turbine [27]. INMET's anemometers measure wind speeds at a height of 10 m. To synchronize the measurements with the wind turbine's hub height of 84 m, an adjustment was implemented using the logarithm law and power law. Considering h the height, h_{ref} the reference measurement height, v_{ref} the wind speed at the reference height and z_0 the roughness length, the vertical variation in wind speed, specifically tailored for a given terrain condition is determined by:

$$v(h) = v_{\text{ref}} \frac{\ln\left(\frac{h}{z_o}\right)}{\ln\left(\frac{h_{\text{ref}}}{z_o}\right)} \tag{4.13}$$

In order to understand the presence of trends in the data set, and estimate the inclination of a linear trend, the non-parametric methods of Mann-Kendall and Sen were applied. Then, a histogram with the occurrences of each value of wind speed was used to calculate the electricity production. Furthermore, the power curve of the wind turbine model SG 3.4-132 is presented in Figure 4.6. Based on the power curve, the wind turbine's cut-in speed, representing the minimum wind speed for electricity generation, is approximately 1.5 m/s. As the wind speed rises, there is a corresponding increase in power. However, beyond the rated wind speed of 8.76 m/s, the generated power remains constant. The wind turbine operates at its rated power from the rated wind speed up to the cut-out speed, which is 20.7 m/s [18].

As a result of the data analysis, the monthly average wind speed at the heights

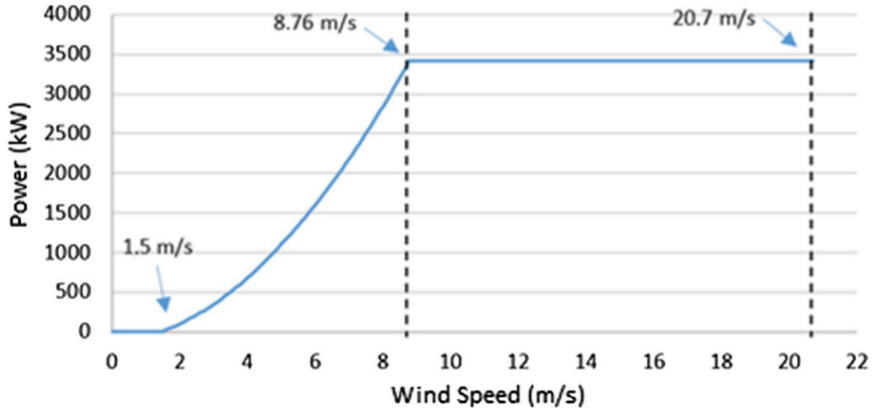

Figure 4.6: Power curve of the turbine SG 3.4-132 [18]

of 10 m and 84 m for both locations is presented in Figure 4.7.

The monthly average wind speeds at 84 m varied between 5.17 and 8.53 m/s for the Patos weather station. Lower wind speeds were observed during the first semester of the year (January to May), ranging from 6.38 to 5.17 m/s. Conversely, the last five months of the year exhibited higher wind speeds, with September and October being particularly significant, reaching values close to 8.50 m/s, in the rated region, between v_r and v_f.

On the other hand, for São Gonçalo, lower average speeds were recorded, fluctuating between 2.41 and 4.40 m/s at the turbine height. It is noteworthy that months with higher wind speeds predominantly occurred in the second semester of the year, similar to the pattern observed for Patos. October emerged as the most notable month, with an average speed approaching 4.40 m/s. In contrast, February, March, and April experienced lower speed values, ranging from 2.41 to 2.58 m/s.

Another interesting metric used was the histogram with the number of occurrences of wind speed values at 84m for both locations, shown in Figure 4.8.

Regarding the annual electricity generation during the studied period in Patos, the years 1998, 2012, 2015, 2016, 2017, and 2018 surpassed the average of the time series. The average, estimated at 18,840 MWh per year with a standard deviation of 4613 MWh, is illustrated in Figure 4.9.Results for electricity generation in São Gonçalo were different. The annual examination of electricity generation reveals that the years 1961, 1962, 1973, 1974, 1975, 1976, 2002, 2016, 2017, and 2018 witnessed wind production exceeding the annual average. The average, estimated at 5556 MWh per year with a standard deviation of 2403 MWh, is depicted in Figure 4.10. Notably, the years 1975, 1976, and 2017 standout with a production 65% higher than the average. Conversely, the years 1963, 1966, 1968, and 1969 exhibited the lowest production, with 1968 being the most significant (approximately 78%

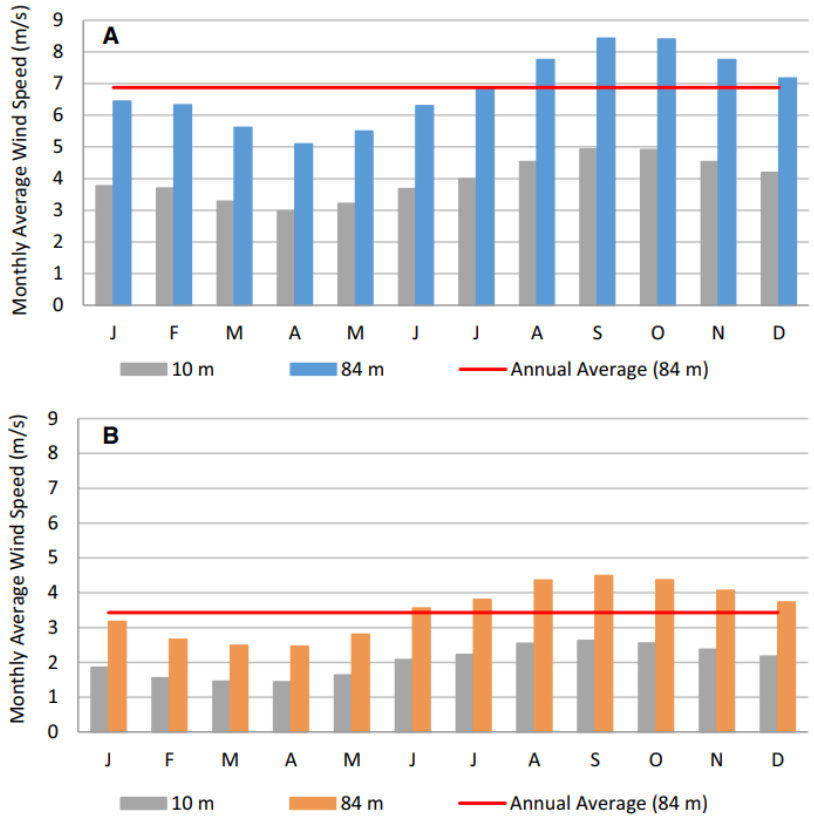

Figure 4.7: Monthly average wind speed at 10 m and 84 m for a Patos station and b São Gonçalo station [18]

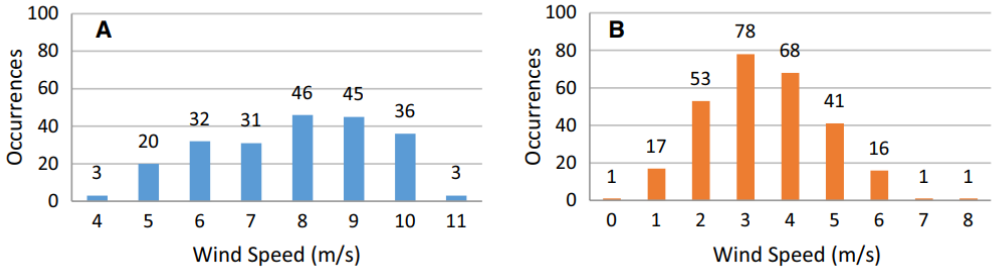

Figure 4.8: Histogram with the number of occurrences of wind speed values at 84 m for: a Patos station from 1977 to 2018 and b São Gonçalo station from 1961 to 2018 [18]

lower than the average).

A monthly study was also carried on in order to analyze wind seasonality and

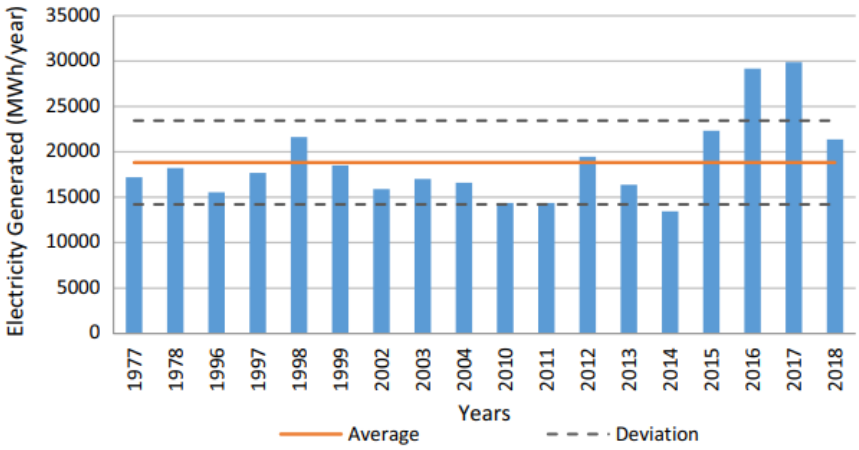

Figure 4.9: Annual electricity generated by the wind turbine SG 3.4–132 from 1977 to 2018 in Patos ($\bar{x}$ = 18,840 MWh/year and =4613 MWh/year)[18]

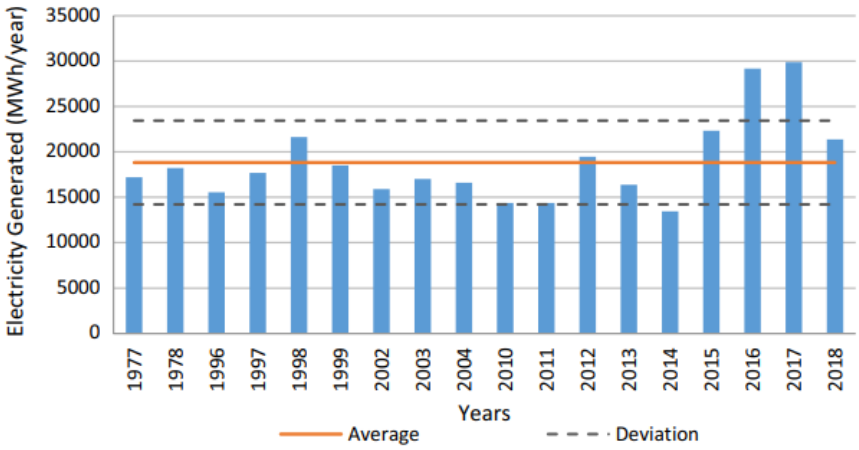

Figure 4.10: Annual electricity generated by the wind turbine SG 3.4–132 from 1961 to 2018 in São Gonçalo ($\bar{x}$ = 5,556 MWh/year and =2403 MWh/year)[18]

predictability, shown in Figures 4.11 and 4.10.

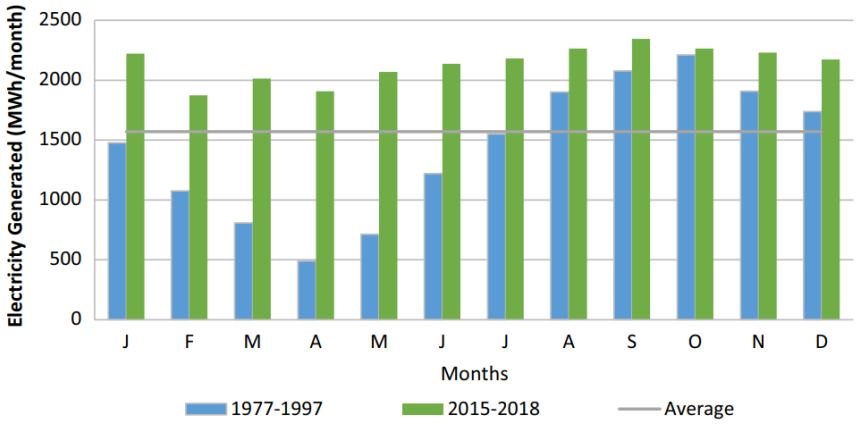

Figure 4.11: Monthly electricity generated by the wind turbine SG 3.4–132 in the frst four years of the time series (1977–1997) and in the last four years (2015–2018) in Patos [18]

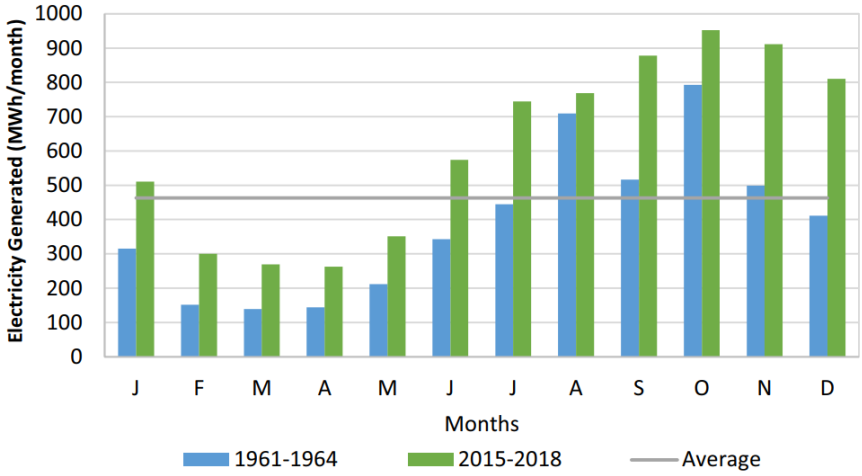

Figure 4.12: Monthly electricity generated by the wind turbine SG 3.4–132 in the frst four years of the time series (1961–1964) and in the last four years (2015–2018) in São Gonçalo [18]

Chapter 5

Study case

The final chapter of this thesis aims to develop a study case based on the concepts of satellite data collection seen in Chapter 3, in order to provide data to be used on the feasibility study of the construction and operation of an offshore wind power plant. The theory seen in Section 4.1, related to wind properties and parameters, will also be applied to verify the feasibility of the site selection. Overall, the key purpose of this investigation is to test the proposed methodology of using satellite data to monitor wind measurements.

Firstly, a study area was defined to fulfill certain requirements. Southeast Brazil is the most populated region of the country, concentrating almost 44% of the country's population, around 203 million in 2022 according to IBGE [28]. The region emerges as a strategic choice for the establishment of energy plants as it presents a compelling case for integration into the energy matrix landscape. Proximity to densely populated urban areas, including major cities like Rio de Janeiro and São Paulo, plays a pivotal role in the region's selection, as it offers a positive scenario for efficient power transmission, reducing energy losses during transportation. Furthermore, the southeast region exhibits a robust and steadily growing demand for energy, driven by its industrial, commercial, and residential sectors. By strategically placing wind power infrastructure in the southeast, it not only meets the regional demand but also aligns with the broader national objective of diversifying the energy mix and reducing dependency on traditional sources. As a result, this geographical positioning, coupled with the region's energy consumption patterns, underscores the feasibility and sustainability of offshore wind power projects in the southeast of Brazil, making it an attractive and viable option for contributing to the nation's renewable energy goals. Particularly in this study, the chosen area is a polygon with longitudes ranging from -42.1736 to -50.4697 and latitudes from -22.4105 to -27.072. By ways of illustration, Aelous provided data, within the mentioned range, in the area shown in Figure 5.1 in June 2022.

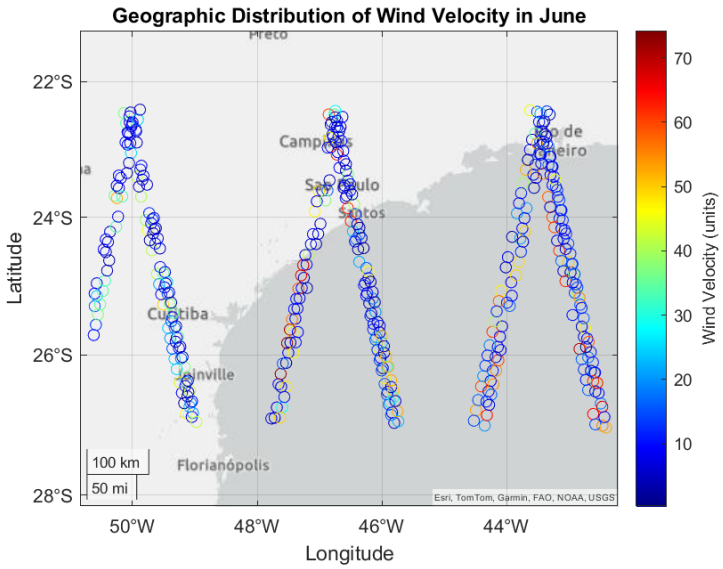

Figure 5.1: Wind velocity map in June 2022

Following the study area selection, the next step was to determine the data source to be used for data collection and analysis among the ones earlier presented, such as EUMETSAT and Aeolus. In this case, the paramount elements in the decision-making process were its reliability and the ease with which data could be downloaded, read and handled, taking into the consideration the availability and coverage of the studied area of southeast Brazil. Even though EUMETSAT had great data accessibility, once downloaded, data could not be easily manipulated as the Add-In indicated for data conversion, MSG Native Image Reader, was malfunctioning. In this scenario, ESA's Earth Explorer Aeolus, shown in Figure 5.2, was a great alternative, specially due to VirES, a highly interactive data manipulation and retrieval interfase for ESA's Aeolus mission products, including tools for studying various atmospheric parameters.

The Aeolus mission provides various publicly accessible products for registered users, including level 1B, level 2A, level 2B and level 2C. The Level 1B data comprises preliminary Horizontal Line of Sight (HLOS) wind observations for both Rayleigh and Mie receivers, featuring standard atmospheric correction for the Rayleigh channel and applied receiver response and bias corrections. In Level 2A, users gain access to a scientific cloud profile product, offering geo-located consolidated backscatter and extinction profiles, along with backscatter-to-extinction and lidar ratio per observation. Additionally, scene classification, scene heterogeneity index, and attenuated backscatter on the measurement level are provided. Level 2B includes a scientific wind product, presenting geo-located

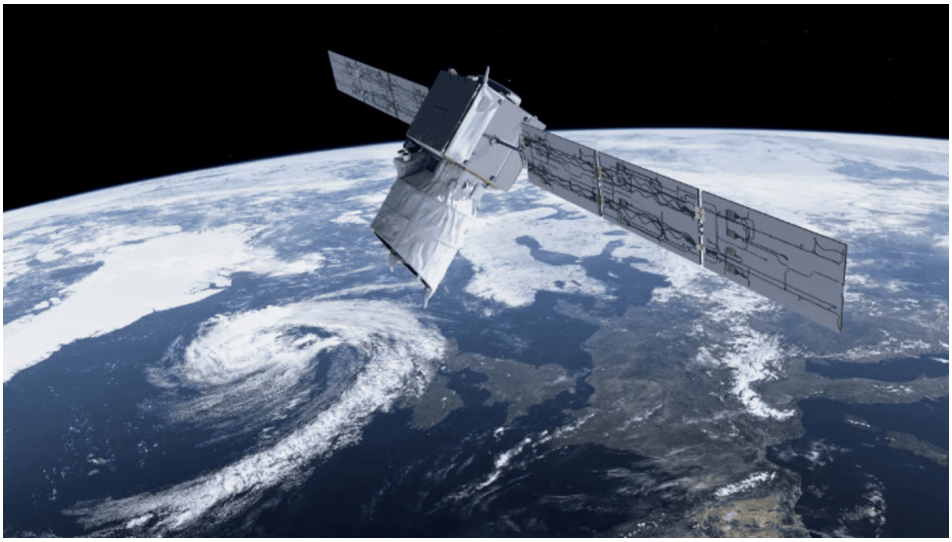

Figure 5.2: ESA's Aeolus satellite

consolidated HLOS wind observations with actual atmospheric correction applied to the Rayleigh channel. Lastly, Level 2C introduces Aeolus-assisted wind fields resulting from Numerical Weather Prediction (NWP) assimilation processing, co-located in time and space with Aeolus wind observations, and generated by the European Centre for Medium-Range Weather Forecasts (ECMWF).

Among the products mentioned, the one chosen for this project was L2C, including Rayleigh wind velocity. In that sense, Rayleigh wind refers to wind observations made using the Rayleigh scattering technique, a method employed in atmospheric remote sensing, particularly in the context of space-based LIDAR systems like the one aboard the Aeolus satellite. The Aeolus satellite, equipped with the Atmospheric Laser Doppler Instrument (Aladin), uses this technique to determine the wind speed by measuring the Doppler shift in the frequency of the scattered light, usually in the lower atmosphere, where air molecules are more abundant. Having chosen the product and the location, the global map shown in Figure 5.3 was obtained.

Aeolus, ESA's Earth Explorer, was launched into space on 22 August 2018 and was retired on 30 April 2023, short before its re-entry on the atmosphere on 28 July. This way, the chosen study period should be compatible with the operation time span, as well as cover all seasons to better evaluate wind conditions. As a result, the analyzed data was collected throughout 2022, from January to December, each month at a time, as VirES only allows downloads of a maximum of 28 days in a row. Within the 28 days, in average Aelous covered the area once a week, every 7 days, as shown in Figure 5.4.

For data analysis, the following steps were executed:

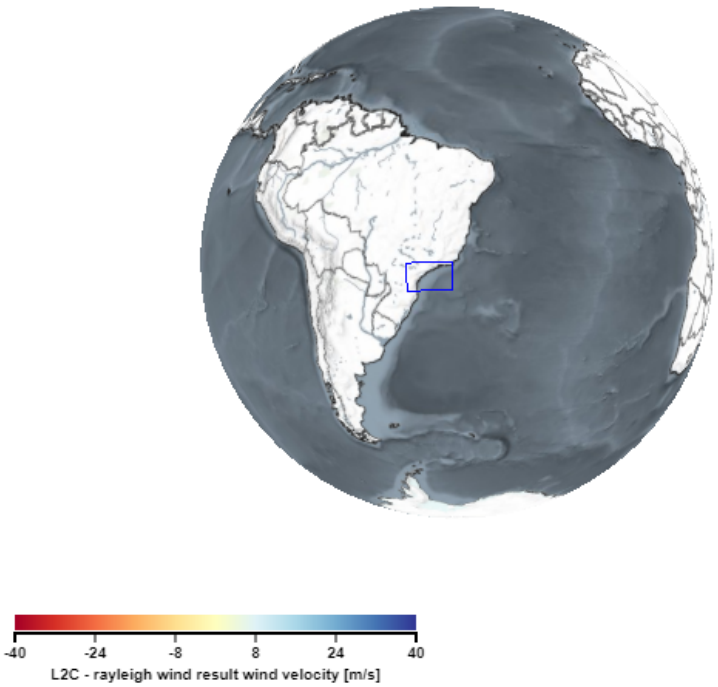

Figure 5.3: Selected area of study on VirES platform

1. Download available monthly data through VirES platform;
2. Utilize Matlab to read .nc file and extract the data, as can be seen in Appendix A;
3. Extract data associated with the variables wind velocity, start time, end time, top altitude, bottom altitude, latitude and longitude;
4. Convert wind velocity from cm/s to m/s;
5. Remove outliers with Matlab's rmoutilers function;
6. Extract statistics for wind velocity such as mean, maximum and minimum value, total range and standard deviation;
7. Define altitude range for a more specific analysis, compatible with the altitudes of an offshore wind turbine;

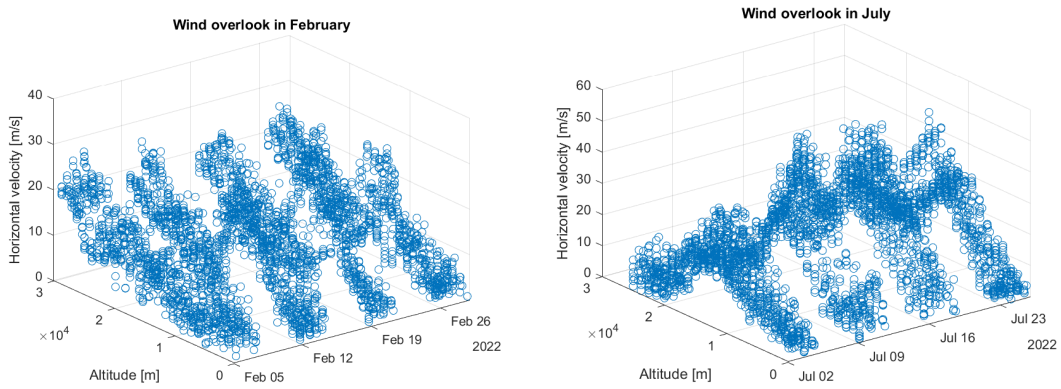

(a) February (b) July

Figure 5.4: Wind overlook with weekly data collection

8. Plot data for better visualization;

9. Utilize Excel for complementary data analysis.

An important initial observation is that the number of measurements made by Aeolus on wind velocity at the studied area varied during the year, specially due to the satellite orbit and trajectory. As seen in Table 5.1, specially in October and November, fewer data was collected, fact also illustrated by Figure 5.5.

Table 5.1: Number of measurements taken by Aelous satellite on the selected area per month

	# for all altitudes	# for altitudes 100-500m	%
Jan/22	3287	92	2.80%
Feb/22	3387	4	0.12%
Mar/22	3332	37	1.11%
Apr/22	3341	65	1.95%
May/22	3235	57	1.76%
Jun/22	3129	51	1.63%
Jul/22	3163	74	2.34%
Aug/22	3010	72	2.39%
Sep/22	3201	65	2.03%
Oct/22	868	19	2.19%
Nov/22	548	2	0.36%
Dec/22	3267	68	2.08%

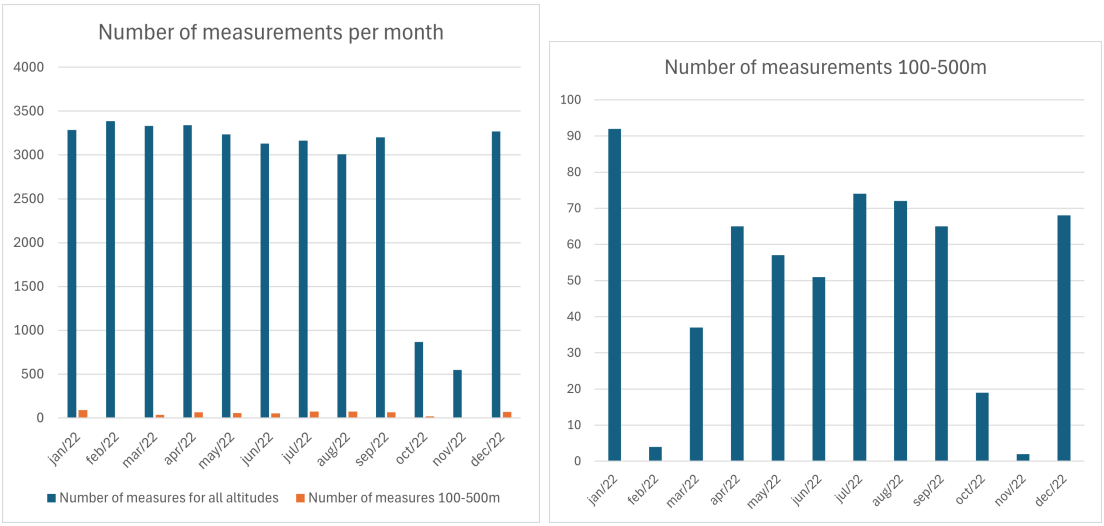

(a) All altitudes

(b) Altitudes from 100-500m

Figure 5.5: Number of wind velocity measurements per month

Furthermore, overall analysis was divided into two main components, the data collected from all altitudes, and the data collected from a specific altitude range. To better visualize how data collection was distributed in terms of altitude, Figure 5.6 shows in which altitudes Aeolus operated in the month of February, the one with the highest number of measurements, 3,387. For this study, the range chosen was between 100m to 500m, compatible in scale to average height of an offshore wind turbine. For instance, the average hub height for offshore wind turbines in the United States is projected to grow from 100 meters in 2016 to about 150 meters in 2035 [29]. At the moment, one of the tallest offshore turbines is GE Renewable Energy's Haliade-X offshore turbine, that boast a height of up to 260 meters.

Using the mentioned methodology, important results associated with average horizontal wind speed were found and shown in Figures 5.7 and 5.8, that also display the standard deviation for each month dataset. As expected, wind velocities rise with altitude due to the studied wind shear effect in chapter 4.1.5, translated in an overall annual mean wind velocity of 14.47 m/s, against 6.63 m/s for altitudes from 100m to 500m. Moreover, although trends were similar, while overall data showed November as the month with weakest winds, for a narrower altitude range, closer to the ground, October was one of the months with weakest winds. That observation, however, contrasts with weather data on southeast Brazil, where October tends to be the month with heavier winds [30]. Standard deviation is also an important parameter to be looked at, and differed considerably between the two scenarios: whilst for a limited altitude range general data dispersion was

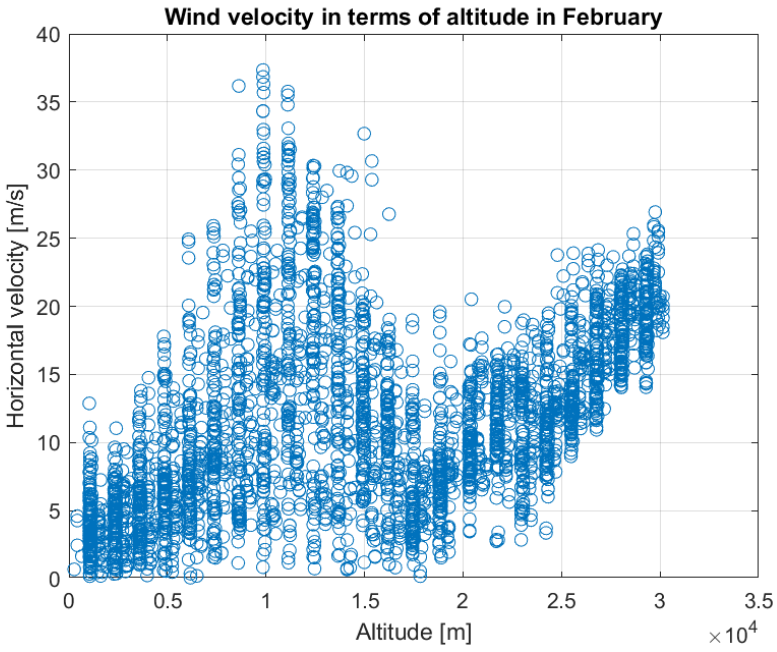

Figure 5.6: Wind velocity in terms of altitude in February 2022

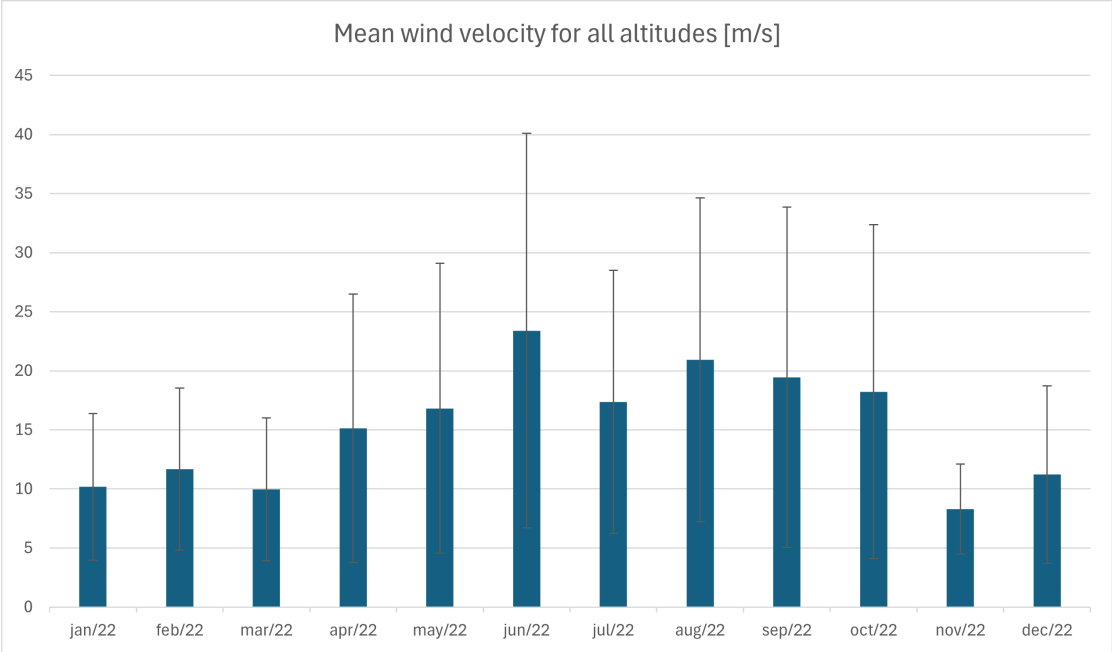

Figure 5.7: Mean horizontal wind velocity throughout 2022 for all altitudes

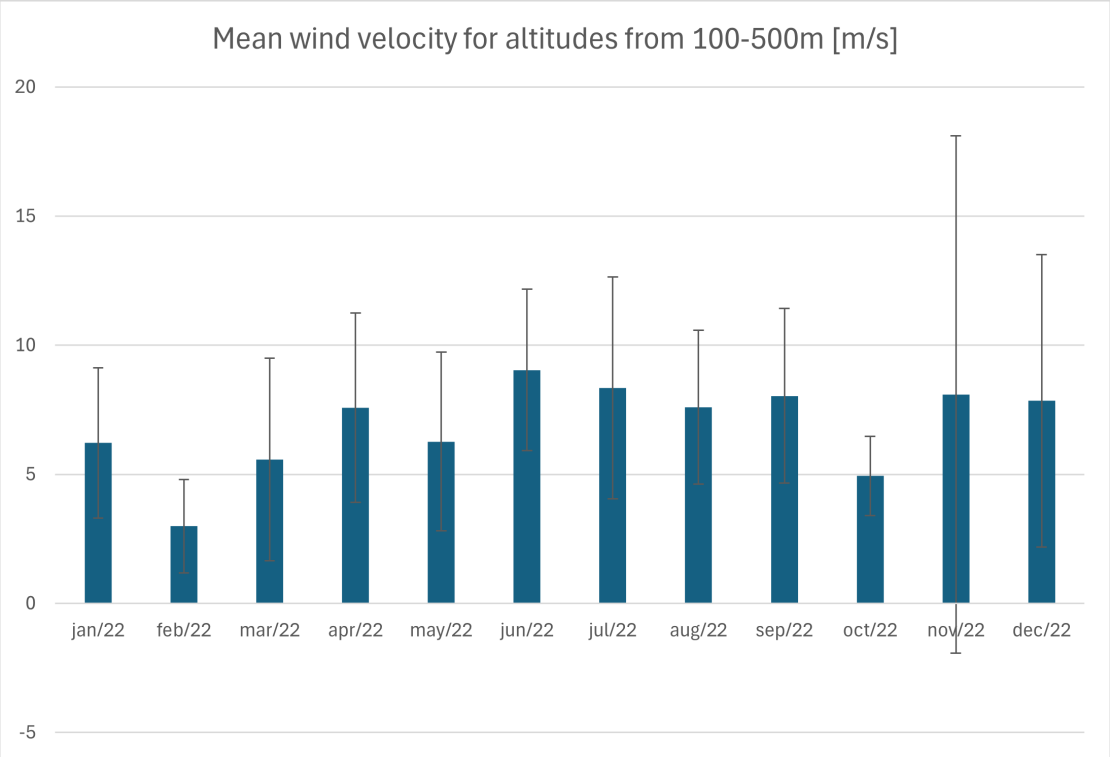

Figure 5.8: Mean horizontal wind velocity throughout 2022 for altitudes from 100m to 500m

unsurprisingly lower, November had a great spike, justified by the considerably low number of measurements made in this month - only 2, as shown in Table 5.1. Considering annual standard deviation instead of the monthly ones, exhibited in Figure 5.8, data deviated 1.657m/s around the mean value of 6.63 m/s.

For a more detailed statistical point of view, Tables 5.3 and 5.2 show secondary information such as minimum and maximum horizontal wind velocities for each month. Notably, minimum velocities were close to zero for all altitudes, contrasting with the maximum ones, that were significantly different in the two scenarios, both in value and occurrence. While maximum velocities reached up to 74 m/s, in June, for all altitudes, the highest value for the 100-500m range was around 22 m/s, in December. February was the month with weakest wind, considering not only mean value, but also range and maximum value, result in line with weather data in southeast Brazil [30].

As a final analysis, aiming to determine latitudes and longitudes with highest horizontal wind velocities within the selected area, simulating a site selection procedure, Figures 5.12 and 5.13 were plotted using Matlab to facilitate the analysis. It is important to punctuated that the pattern visualized in the graph

Table 5.2: Wind velocity statistics for all altitudes [m/s]

	Mean	Std. deviation	Minimum	Maximum	Range
Jan/22	10.184	6.211	0.136	32.887	32.751
Feb/22	11.678	6.865	0.070	37.347	37.277
Mar/22	9.964	6.049	0.184	29.936	29.753
Apr/22	15.134	11.358	0.177	47.997	47.820
May/22	16.817	12.272	0.092	57.172	57.080
Jun/22	23.397	16.688	0.208	74.224	74.016
Jul/22	17.364	11.143	0.160	53.919	53.759
Aug/22	20.932	13.718	0.320	64.949	64.629
Sep/22	19.448	14.395	0.255	63.887	63.632
Oct/22	18.228	14.133	0.067	57.571	57.504
Nov/22	8.292	3.816	0.135	18.945	18.811
Dec/22	11.213	7.510	0.117	34.869	34.752

Table 5.3: Wind velocity statistics for altitudes from 100-500m [m/s]

	Mean	Std. deviation	Minimum	Maximum	Range
Jan/22	6.218	2.911	0.559	12.667	12.108
Feb/22	2.999	1.810	0.683	4.595	3.912
Mar/22	5.575	3.915	0.554	12.941	12.387
Apr/22	7.584	3.661	0.995	16.954	15.959
May/22	6.265	3.461	1.446	14.142	12.696
Jun/22	9.041	3.132	3.564	16.850	13.287
Jul/22	8.351	4.300	0.228	17.615	17.387
Aug/22	7.606	2.981	0.320	15.375	15.055
Sep/22	8.036	3.380	1.480	14.795	13.315
Oct/22	4.941	1.535	2.270	7.235	4.965
Nov/22	8.097	10.021	1.011	15.183	14.171
Dec/22	7.850	5.660	0.382	22.758	22.376

reflects Aeolus trajectory and coverage in the selected area for all altitudes. From the images, it can be inferred that wind velocities vary more according to longitude than latitude, as seen specially in the months of March, April, June and July. Throughout the year, it can also be seen that higher longitudes, further from the coastline, tends to have higher wind velocities.

In addition, for a 3D display considering also the altitudes for which each data was collected, Figures 5.14 and 5.15 are shown.

Following the data analysis, a next step would be to simulate the operation of a offshore wind farm in the selected location based on the wind speeds found. In

order to do that, the following steps were took:

1. Build a probability density function through Matlab;
2. Set a suitable turbine to be used for the analysis;
3. Draw the power curve for the selected turbine;
4. Define the power output given the wind speed probability density function;
5. Estimate the revenue for a single turbine given the weather conditions extracted from satellite data.

The goal of building a probability density function is to determine the occurrence and frequency of different values amongst a set of measurements. In this study, as data is not continuously collected by satellites, a discrete pattern was considered and a frequency distribution table was built to calculate the occurrence of certain velocity ranges, with the output given by Figure 5.9.

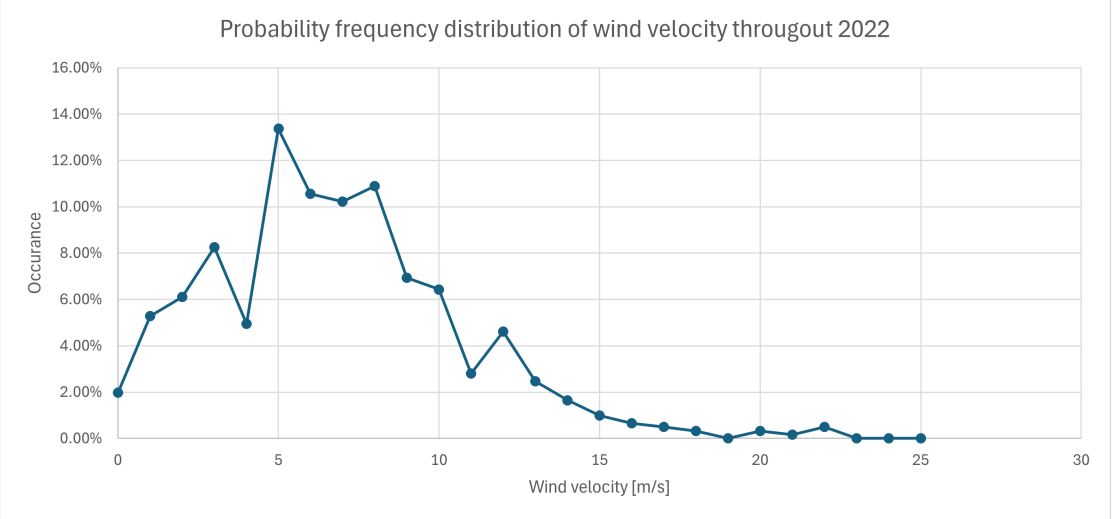

Figure 5.9: Probability frequency distribution for wind velocity throughout 2022

A powerful tool to be used in a similar analysis would be the Weibull distribution, a continuous probability distribution widely used in areas such as reliability engineering and wind energy, as it provides model wind speed distributions at a specific location. Considering x the random variable (wind speed), k the shape parameter, λ the scale parameter, the probability density function (PDF) of the Weibull distribution is given by equation 5.1. Considering $\lambda = 7.5$ and $k = 3.5$, the distribution is depicted in Figure 5.10.

$$f(x;\lambda,k) = \frac{k}{\lambda}\left(\frac{x}{\lambda}\right)^{k-1} e^{-(x/\lambda)^k} \tag{5.1}$$

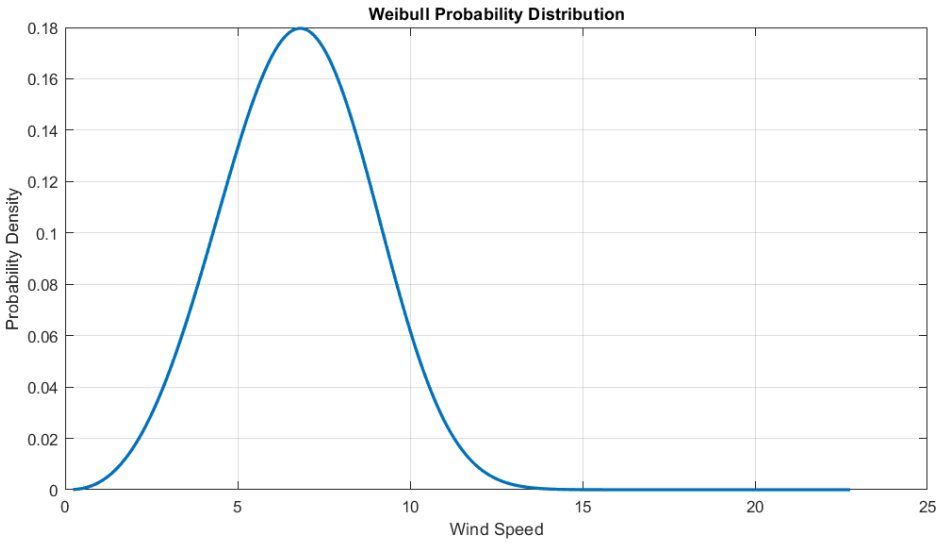

Figure 5.10: Weibull distribution function for wind velocity throughout 2022

Following the design of the two probability density functions, the next step would be to define a suitable turbine for the study. In the same manner the research shown in Chapter 4.2 chose the turbine model SG 3.4-132, adequate for onshore conditions, in order to draw a parallel between the two studies, the wind turbine Siemens Gamesa SG 14-222 DD was selected. Characterized for being a 14 MW offshore wind turbine which delivers high production of sustainable energy at all wind conditions, it also presents a rotor diameter of 222 meters, compatible to the altitude range (100m - 500m) used to refine the satellite data collected. Considering the turbine's datasheet, including its cut-in speed (3 m/s), rated wind speed (12 m/s) and cut-out speed (32 m/s), the following power curve was drawn using a cubic function to represent the relationship between the wind speed and the power output. This is based on the principle that power extracted from the wind is proportional to the cube of the wind speed, as long as the turbine is operating below its rated power, as depicted in equation 4.2.

Once the power curve is known, it is possible to define the power output to each given velocity range. That way, the estimated power produced by a turbine could be measured by the following equation, where fr_i is the frequency of each power output P_i:

$$EP = \sum fr_i \times P_i \tag{5.2}$$

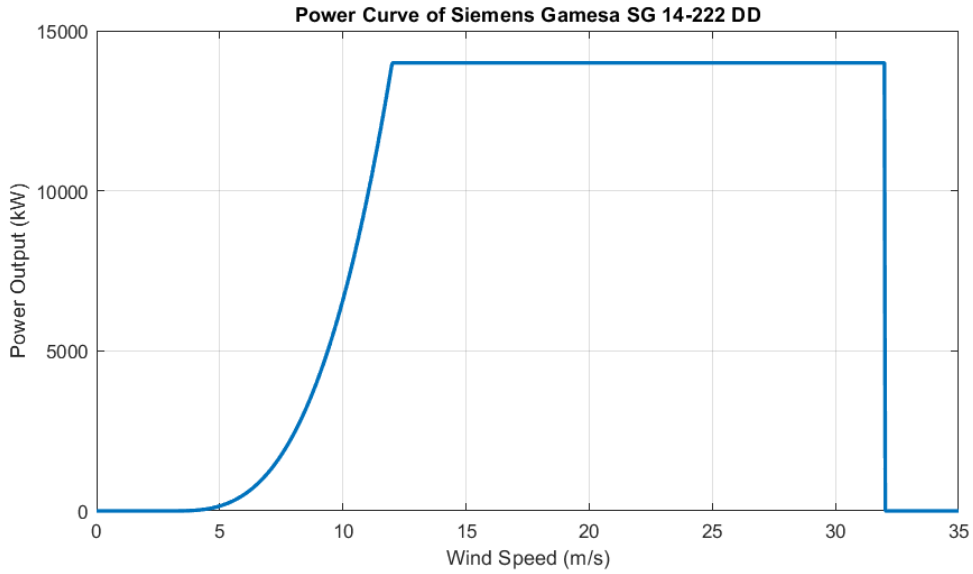

Figure 5.11: Power curve of the turbine Siemens Gamesa SG 14-222 DD

Considering the discrete distribution function, on Table 5.4, the forth column displays the power produced by the turbine for a certain velocity given its frequency. One observation to be made is that in this study, as the turbine's rated wind speed is 12 m/s, on 12.21% of the time the satellite collected data the turbine would be operating on its maximum output capacity. On a further analysis, to calculate the total power generated per year, based solely on data collected in 2022, the sum of all TPs is multiplied by the number of hours in a year with 365 days such as 2022 (8,760). Hence, the total per year can be estimated in $3{,}584.86 \times 8{,}760 = 31{,}403.37$ MWh/year.

Applying the same process, but this time based on Weibull distribution, Table 5.5 was found. For this scenario, the outcome was a significantly lower energy production when compared to the previous number, as 1,998.55 kW represents only 55.75% of the total result given by Table 5.4. Consequently, the total energy produced by the turbine in a year would be $1{,}998.55 \times 8{,}760 = 17{,}507.30$ MWh/year.

To guide the decision over the economic viability of a project involving the construction and operation of offshore wind power plants in southeast Brazil, a important parameter is the wind power sales price, stipulated by Agência Nacional de Energia Elétrica (ANEEL), the Brazilian Electricity Regulatory Agency. Its main responsibilities include regulating and supervising the generation, transmission, distribution, and commercialization of electric energy in Brazil, being also responsible for setting the rules and tariffs for the electricity sector. The price of

Wind Velocity [m/s]	Freq. [%]	Output Power [kW]	Freq. x Power [kW]
0-1	1.98%	0.00	0.00
1-2	5.28%	0.00	0.00
2-3	6.11%	0.00	0.00
3-4	8.25%	2.40	0.20
4-5	4.95%	64.80	3.21
5-6	13.37%	300.10	40.11
6-7	10.56%	823.40	86.96
7-8	10.23%	1,750.00	179.04
8-9	10.89%	3,195.10	347.98
9-10	6.93%	5,274.00	365.52
10-11	6.44%	8,101.90	521.41
11-12	2.81%	11,793.90	330.85
12-13	4.62%	14,000.00	646.86
13-14	2.48%	14,000.00	346.53
14-15	1.65%	14,000.00	231.02
15-16	0.99%	14,000.00	138.61
16-17	0.66%	14,000.00	92.41
17-18	0.50%	14,000.00	69.31
18-19	0.33%	14,000.00	46.20
19-20	0.00%	14,000.00	0.00
20-21	0.33%	14,000.00	46.20
21-22	0.17%	14,000.00	23.10
22-23	0.50%	14,000.00	69.31
23-24	0.00%	14,000.00	0.00
24-25	0.00%	14,000.00	0.00
Total [kW]			3,584.86

Table 5.4: Frequency distribution table of wind velocity and corresponding power output

wind energy in Brazil is typically determined through competitive auctions conducted by ANEEL. In these auctions, companies bid to supply a certain amount of energy at a specified price (in Brazilian Reais per megawatt-hour, MWh). ANEEL then awards contracts to the winning bidders based on their proposed prices and other criteria such as project feasibility and environmental sustainability.

On September 2022, ANEEL approved a new guideline for the auctioning of clean energy, the A-5. In it, it is stated that the initial prices for plants without permits and with permits but without contract is R$ 280,00/MWh for solar and

Wind Velocity [m/s]	Freq. [%]	Output Power [kW]	Freq. x Power [kW]
0-1	0.09%	0.00	0.00
1-2	0.89%	0.00	0.00
2-3	2.99%	0.00	0.00
3-4	6.52%	2.40	0.156
4-5	11.00%	64.80	7.129
5-6	15.25%	300.10	45.775
6-7	17.67%	823.40	145.474
7-8	17.04%	1,750.00	298.170
8-9	13.49%	3,195.10	430.998
9-10	8.59%	5,274.00	452.878
10-11	4.29%	8,101.90	347.173
11-12	1.63%	11,793.90	192.090
12-13	0.46%	14,000.00	63.968
13-14	0.09%	14,000.00	12.805
14-15	0.01%	14,000.00	1.764
15-16	0.00%	14,000.00	0.161
16-17	0.00%	14,000.00	0.009
17-18	0.00%	14,000.00	0.000
18-19	0.00%	14,000.00	0.000
19-20	0.00%	14,000.00	0.000
20-21	0.00%	14,000.00	0.000
21-22	0.00%	14,000.00	0.000
22-23	0.00%	14,000.00	0.000
23-24	0.00%	14,000.00	0.000
24-25	0.00%	14,000.00	0.000
Total [kW]			1,998.55

Table 5.5: Frequency distribution table of wind velocity and corresponding power output considering the Weibull distribution function

wind energy. On the other hand, for projects with a grant and a contract, the price for wind energy changes to R$ 212,37/MWh [31]. Considering the first scenario and a discrete frequency wind velocity distribution, the 31,403.37 MWh/year produced by a single turbine SG 14-222 DD in the selected area could be sold for $31{,}403.37 \times 280{,}00 =$ R$ 8,792,942.75 per year. On the other hand, taking into account the Weibull distribution, the energy could be sold for $17{,}507.30 \times 280{,}00 =$ R$ 4,902,043.44.

A relevant final observation to be made is that in order to evaluate the total

amount of energy generated, and thus the total revenue to be considered for an entire power plant with multiple turbines, the wake effects mentioned in Section 4.1.2 would have to be examined, as they would impact power generation by reducing the wind speed of a downwind turbine, as seen in Figure 4.3.

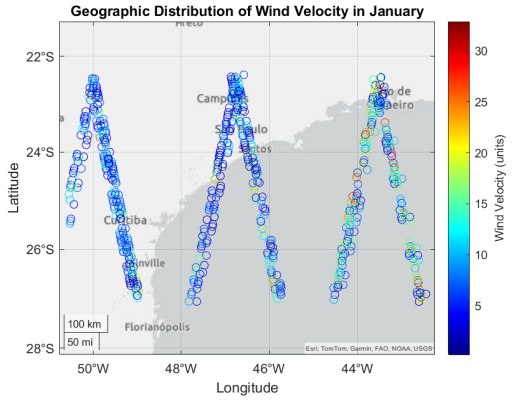

(a) January

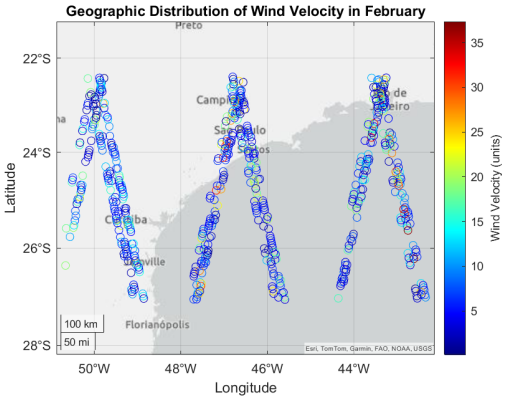

(b) February

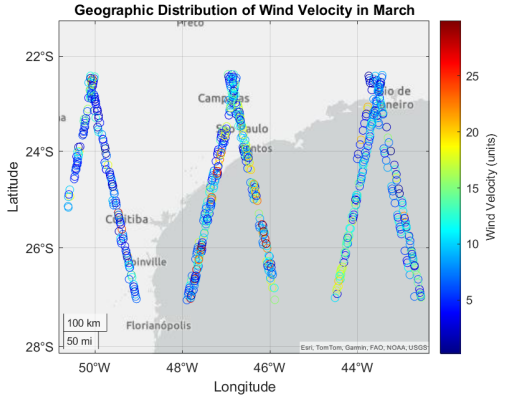

(c) March

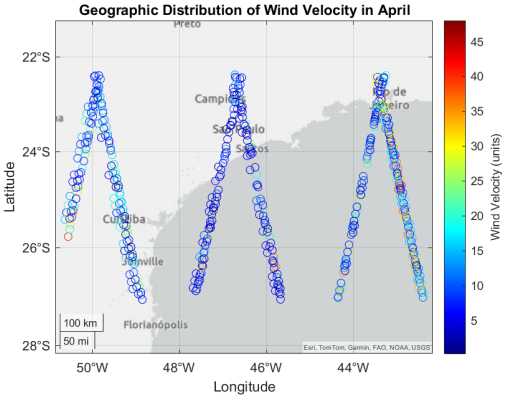

(d) April

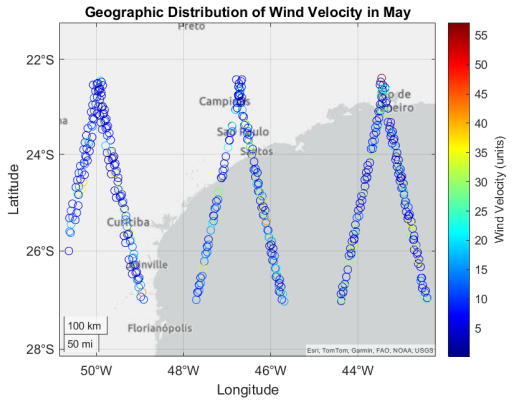

(e) May

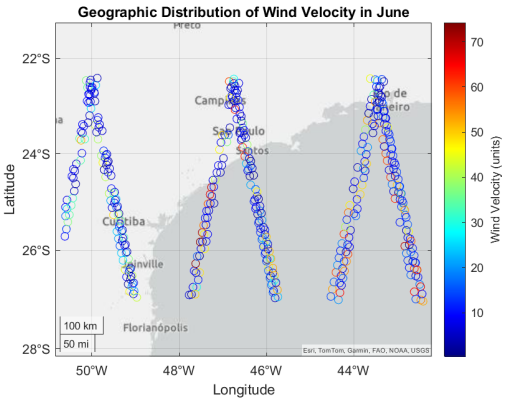

(f) June

Figure 5.12: Wind velocity geographical distribution January - June 2022

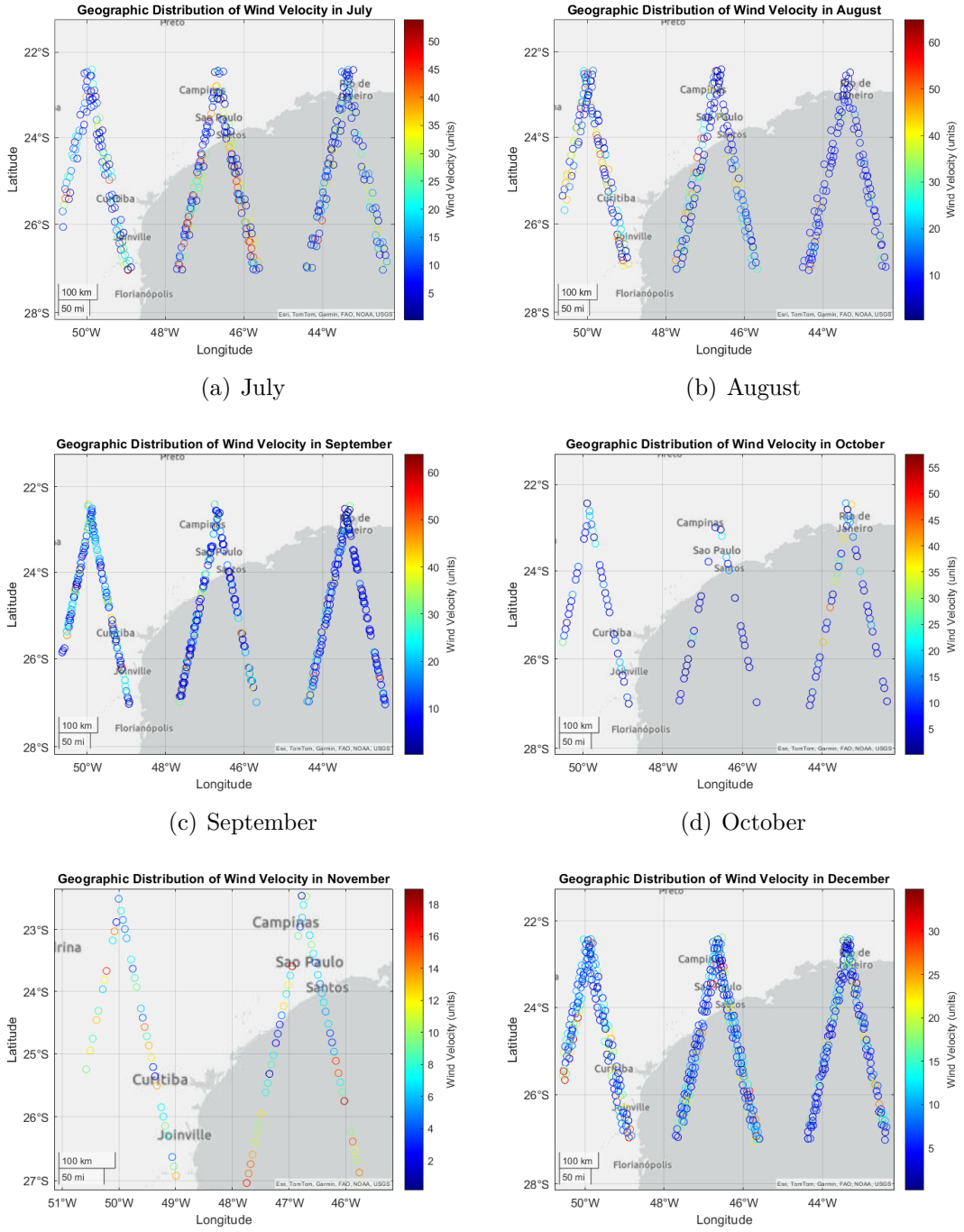

(a) July (b) August

(c) September (d) October

(e) November (f) December

Figure 5.13: Wind velocity geographical distribution July - December 2022

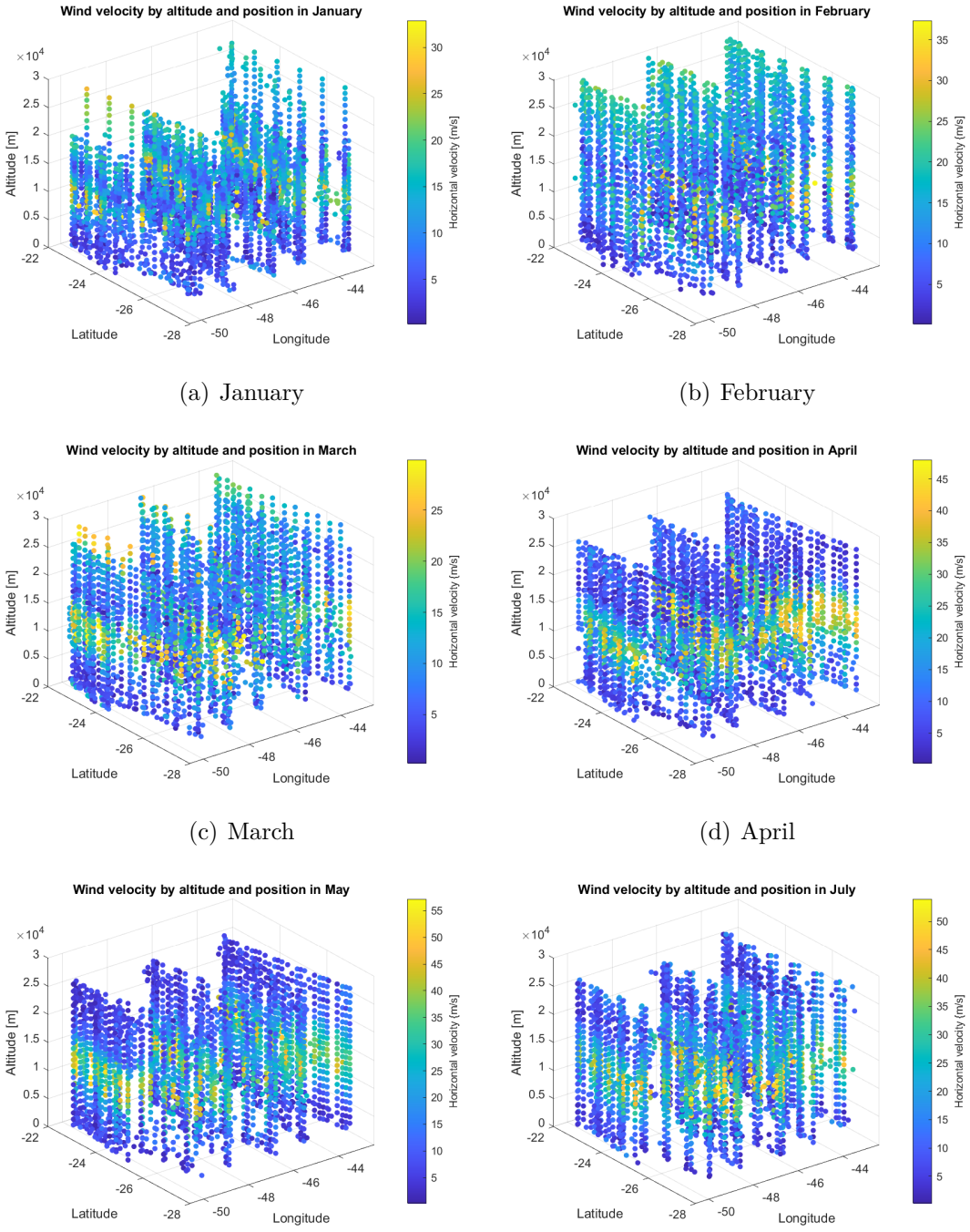

(a) January

(b) February

(c) March

(d) April

(e) May

(f) June

Figure 5.14: Wind velocity distribution from January to June 2022 considering altitude, latitude and longitude

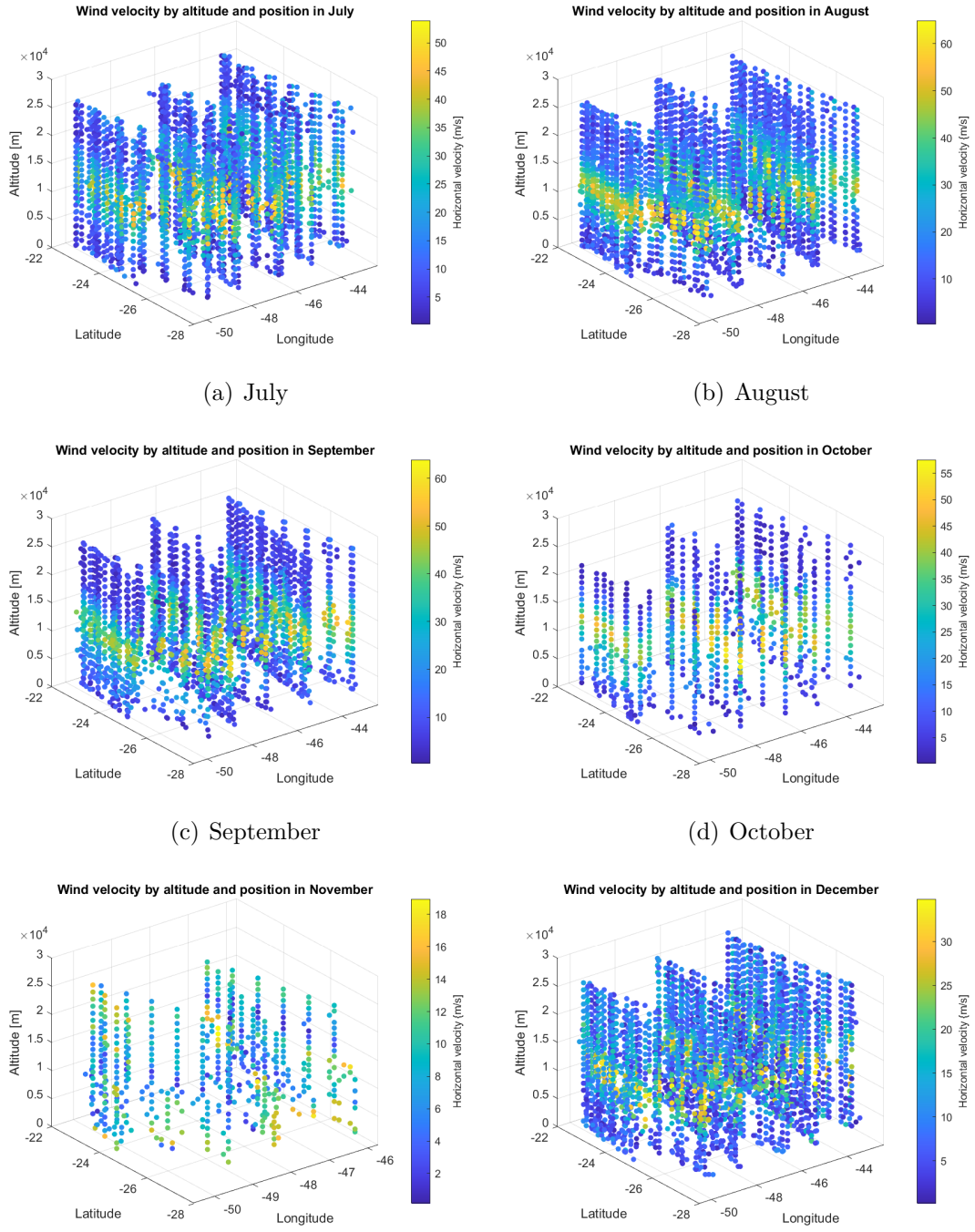

(a) July

(b) August

(c) September

(d) October

(e) November

(f) December

Figure 5.15: Wind velocity distribution from July to December 2022 considering altitude, latitude and longitude

Chapter 6

Conclusion

To draw a conclusion whether the employed methodology was successful, more important than the results is to determine the reliability of the selected data source. The goal of this thesis was to study the feasibility of using satellite data to monitor the construction and operation of offshore wind power plants, comprising of, in the Brazilian context, also the licensing phase. For that, many satellite data sources were mentioned and briefly detailed, prior to choosing Aelous as the main data source.

In general, using satellite data complementary to in-situ measurements allows for a more comprehensive assessment of wind patterns across large offshore areas, which helps in identifying optimal locations for wind farm deployment and understanding regional wind characteristics. Compared to on-site measurements, it has the advantage of not needing extensive fieldwork or infrastructure in order to collect data, although there could be limitations in data coverage due to the spacecraft trajectory. Additionally, it is capable of developing long-term, consistent records of wind patterns over large spatial scales, enabling assessing long-term trends and variability in wind resources.

Aelous, specifically, besides the mentioned advantages, presented great ease of use, allowing data access through a platform with good interface and usage instructions. Nevertheless, some constraints were found. For instance, the time span of only 28 days for each download created a longer process for collecting data over a year long period. As the satellite operated from August 2018 to April 2023, data could only be found within that range. Furthermore, as the satellite follows a certain trajectory, the measurements did not cover the totality of the selected area, but a zig zag pattern over the chosen rectangular area, as seen in Figures 5.14 and 5.15. Lastly, as discussed in the section 1.2, fewer data was available in lower altitudes, with also some variability throughout the year as some months, like October and November, presented less measurements.

Based solely on the results found by Aelous data collected in 2022, a single SG

14-222 DD turbine on the selected area of study presented potential of generating R$ 8,792,942.75 per year, roughly 1,584,321.57€ considering the Foreign Exchange spot rate on April 25th, 2024. To verify the economic viability of such project, a further study on the total annual cost for the construction and operation of the wind farm, shaped by the number of turbines to be installed, and wake effect implications would have to be conducted. A next important step in this study would also be to reconsider the feasibility of the selected area for the operation of offshore wind power plants if in-site measurements were contemplated, as well as expanding the time span of the selected data. Moreover, a smaller area of study could be picked out considering the zones with higher wind velocities and lower standard deviation, possibly achieving better wind conditions upon a further study.

Overall, integrating satellite data with in-situ wind measurements enhances the accuracy, reliability, and efficiency of monitoring offshore wind power plants, ultimately supporting the sustainable development and management of offshore wind energy resources. The methodology introduced on this thesis, with the usage of Aelous data to determine the feasibility of the construction and operation of offshore wind power plants, proved to be valuable tool in the decision-making process, in particular when aligned with on site measurements.

Appendix A

Appendix A - Matlab Code

```
% Read download file

close all
clear all
clc

%%

monthn = 1; %period of data collection; 1 for January ... 12 for
    Decembe11

if monthn == 1
     month = 'January';
     ncdisp("C:\Users\gabiv\OneDrive\Área de Trabalho\POLITO - Space
    Economy\Thesis\Dados\Aeolus\Matlab\
    AE_OPER_ALD_U_N_2C_public_20220102T024256_20220129T235959_vires.nc
    "); %jan
     ncfile = 'C:\Users\gabiv\OneDrive\Área de Trabalho\POLITO - Space
     Economy\Thesis\Dados\Aeolus\Matlab\
    AE_OPER_ALD_U_N_2C_public_20220102T024256_20220129T235959_vires.nc
    '; % jan
elseif monthn == 2
     month = 'February';
     ncdisp("C:\Users\gabiv\OneDrive\Área de Trabalho\POLITO - Space
    Economy\Thesis\Dados\Aeolus\Matlab\
    AE_OPER_ALD_U_N_2C_public_20220201T024256_20220228T235959_vires.nc
    "); %feb
     ncfile = 'C:\Users\gabiv\OneDrive\Área de Trabalho\POLITO - Space
     Economy\Thesis\Dados\Aeolus\Matlab\
    AE_OPER_ALD_U_N_2C_public_20220201T024256_20220228T235959_vires.nc
    '; % feb
```

```
elseif monthn == 3
    month = 'March';
    ncdisp("C:\Users\gabiv\OneDrive\Área de Trabalho\POLITO - Space Economy\Thesis\Dados\Aeolus\Matlab\AE_OPER_ALD_U_N_2C_public_20220302T024256_20220329T235959_vires.nc"); %mar
    ncfile = 'C:\Users\gabiv\OneDrive\Área de Trabalho\POLITO - Space Economy\Thesis\Dados\Aeolus\Matlab\AE_OPER_ALD_U_N_2C_public_20220302T024256_20220329T235959_vires.nc'; % mar
elseif monthn == 4
    month = 'April';
    ncdisp("C:\Users\gabiv\OneDrive\Área de Trabalho\POLITO - Space Economy\Thesis\Dados\Aeolus\Matlab\AE_OPER_ALD_U_N_2C_public_20220402T024256_20220429T235959_vires.nc"); %apr
    ncfile = 'C:\Users\gabiv\OneDrive\Área de Trabalho\POLITO - Space Economy\Thesis\Dados\Aeolus\Matlab\AE_OPER_ALD_U_N_2C_public_20220402T024256_20220429T235959_vires.nc'; % apr
elseif monthn == 5
    month = 'May';
    ncdisp("C:\Users\gabiv\OneDrive\Área de Trabalho\POLITO - Space Economy\Thesis\Dados\Aeolus\Matlab\AE_OPER_ALD_U_N_2C_public_20220502T024256_20220529T235959_vires.nc"); %may
    ncfile = 'C:\Users\gabiv\OneDrive\Área de Trabalho\POLITO - Space Economy\Thesis\Dados\Aeolus\Matlab\AE_OPER_ALD_U_N_2C_public_20220502T024256_20220529T235959_vires.nc'; %may
elseif monthn == 6
    month = 'June';
    ncdisp("C:\Users\gabiv\OneDrive\Área de Trabalho\POLITO - Space Economy\Thesis\Dados\Aeolus\Matlab\AE_OPER_ALD_U_N_2C_public_20220602T024256_20220629T235959_vires.nc"); %jun
    ncfile = 'C:\Users\gabiv\OneDrive\Área de Trabalho\POLITO - Space Economy\Thesis\Dados\Aeolus\Matlab\AE_OPER_ALD_U_N_2C_public_20220602T024256_20220629T235959_vires.nc'; %jun
elseif monthn == 7
    month = 'July';
    ncdisp("C:\Users\gabiv\OneDrive\Área de Trabalho\POLITO - Space Economy\Thesis\Dados\Aeolus\Matlab\AE_OPER_ALD_U_N_2C_public_20220702T024256_20220729T235959_vires.nc"); %jul
```

```
38      ncfile = 'C:\Users\gabiv\OneDrive\Área de Trabalho\POLITO - Space
        Economy\Thesis\Dados\Aeolus\Matlab\
    AE_OPER_ALD_U_N_2C_public_20220702T024256_20220729T235959_vires.nc
    '; %jul
39  elseif monthn == 8
40      month = 'August';
41      ncdisp("C:\Users\gabiv\OneDrive\Área de Trabalho\POLITO - Space
    Economy\Thesis\Dados\Aeolus\Matlab\
    AE_OPER_ALD_U_N_2C_public_20220802T024256_20220829T235959_vires.nc
    "); %aug
42      ncfile = 'C:\Users\gabiv\OneDrive\Área de Trabalho\POLITO - Space
        Economy\Thesis\Dados\Aeolus\Matlab\
    AE_OPER_ALD_U_N_2C_public_20220802T024256_20220829T235959_vires.nc
    '; %aug
43  elseif monthn == 9
44      month = 'September';
45      ncdisp("C:\Users\gabiv\OneDrive\Área de Trabalho\POLITO - Space
    Economy\Thesis\Dados\Aeolus\Matlab\
    AE_OPER_ALD_U_N_2C_public_20220902T024256_20220929T235959_vires.nc
    "); %sep
46      ncfile = 'C:\Users\gabiv\OneDrive\Área de Trabalho\POLITO - Space
        Economy\Thesis\Dados\Aeolus\Matlab\
    AE_OPER_ALD_U_N_2C_public_20220902T024256_20220929T235959_vires.nc
    '; %sep
47  elseif monthn == 10
48      month = 'October';
49      ncdisp("C:\Users\gabiv\OneDrive\Área de Trabalho\POLITO - Space
    Economy\Thesis\Dados\Aeolus\Matlab\
    AE_OPER_ALD_U_N_2C_public_20221001T024256_20221028T235959_vires.nc
    "); %oct
50      ncfile = 'C:\Users\gabiv\OneDrive\Área de Trabalho\POLITO - Space
        Economy\Thesis\Dados\Aeolus\Matlab\
    AE_OPER_ALD_U_N_2C_public_20221001T024256_20221028T235959_vires.nc
    '; %oct
51  elseif monthn == 11
52      month = 'November';
53      ncdisp("C:\Users\gabiv\OneDrive\Área de Trabalho\POLITO - Space
    Economy\Thesis\Dados\Aeolus\Matlab\
    AE_OPER_ALD_U_N_2C_public_20221102T024256_20221129T235959_vires.nc
    "); %nov
54      ncfile = 'C:\Users\gabiv\OneDrive\Área de Trabalho\POLITO - Space
        Economy\Thesis\Dados\Aeolus\Matlab\
    AE_OPER_ALD_U_N_2C_public_20221102T024256_20221129T235959_vires.nc
    '; %nov
55  elseif monthn == 12
56      month = 'December';
```

```
57      ncdisp("C:\Users\gabiv\OneDrive\Área de Trabalho\POLITO - Space
        Economy\Thesis\Dados\Aeolus\Matlab\
        AE_OPER_ALD_U_N_2C_public_20221202T024256_20221229T235959_vires.nc
        "); %dec
58      ncfile = 'C:\Users\gabiv\OneDrive\Área de Trabalho\POLITO - Space
         Economy\Thesis\Dados\Aeolus\Matlab\
        AE_OPER_ALD_U_N_2C_public_20221202T024256_20221229T235959_vires.nc
        '; %dec
59  end
60
61  variable_name = ["
        rayleigh_assimilation_analysis_horizontal_wind_velocity","
        rayleigh_wind_result_stop_time","rayleigh_wind_result_start_time",
        "rayleigh_wind_result_top_altitude","
        rayleigh_wind_result_bottom_altitude","
        rayleigh_assimilation_analysis_wind_direction","
        rayleigh_wind_result_lon_of_DEM_intersection","
        rayleigh_wind_result_lat_of_DEM_intersection"]; %variable that you
         want
62
63  folderPath = 'C:\Users\gabiv\OneDrive\Área de Trabalho\POLITO - Space
         Economy\Thesis\Imagens\MATLAB'; %where the images generated by
        matlab will be saved in
64
65
66  groupname = 'rayleigh_wind_data';
67
68  % The loop is useful to extract more variables quickly. i is the
        number of variables you want to extract.
69
70  for i = 1:8
71      ncid = netcdf.open(ncfile, 'NOWRITE');
72
73  % Get the group ID
74      groupid = netcdf.inqNcid(ncid, groupname);
75
76  % List the variables within the group
77  % varnames = netcdf.inqVarNames(groupid);
78
79       variable_name_2 = variable_name{1,i};
80       varid = netcdf.inqVarID(groupid,variable_name_2);
81
82  % Read the variable data
83      data = netcdf.getVar(groupid, varid);
84
85  % Close the NetCDF file when done
86      netcdf.close(ncid);
87
88      if i == 1
```

```
89          wind_velocity = data;
90      elseif i == 2
91          stop_time = data;
92      elseif i == 3
93          start_time = data;
94      elseif i == 4
95          top_altitude = data;
96      elseif i == 5
97          bottom_altitude = data;
98      elseif i == 6
99          wind_direction = data;
100     elseif i == 7
101         wind_longitude = data;
102     elseif i == 8
103         wind_latitude = data;
104     end
105 end
106
107
108 %%
109
110 % 11 seconds is the radar acquisition window
111
112 mean_altitude = (bottom_altitude + top_altitude)./2;
113
114 mean_time = (stop_time + start_time)/2;
115
116 wind_velocity_ms = wind_velocity/100; %convert from      /s to m/s
117
118 % Identify and remove outliers in wind_velocity
119 [wind_velocity_cleaned, idx_outliers] = rmoutliers(wind_velocity_ms);
120
121 % Statistics for wind velocity
122 mean_wind_all_alt = mean(wind_velocity_cleaned);
123 min_wind_all_alt = min(wind_velocity_cleaned);
124 max_wind_all_alt = max(wind_velocity_cleaned);
125 range_wind_all_alt = range(wind_velocity_cleaned);
126 std_wind_all_alt = std(wind_velocity_cleaned);
127 all_alt_stats = {
128     'Mean wind for all altitudes', mean_wind_all_alt;
129     'Minimum wind for all altitudes', min_wind_all_alt;
130     'Maximum wind for all altitudes', max_wind_all_alt;
131     'Range of wind for all altitudes', range_wind_all_alt;
132     'Standard deviation for all altitudes', std_wind_all_alt;
133     };
134
135 % Remove corresponding elements from mean_time and mean_altitude
136 mean_time_cleaned = mean_time;
137 mean_time_cleaned(idx_outliers) = [];
```

```
mean_altitude_cleaned = mean_altitude;
mean_altitude_cleaned(idx_outliers) = [];
wind_latitude_cleaned = wind_latitude;
wind_latitude_cleaned(idx_outliers) = [];
wind_longitude_cleaned_1 = wind_longitude;
wind_longitude_cleaned_1(idx_outliers) = [];
wind_longitude_cleaned = wind_longitude_cleaned_1 - 360;

reference_time = datetime('2000-01-01 00:00:00', 'Format', 'yyyy-MM-
    dd HH:mm:ss', 'TimeZone', 'UTC');

time_in_datetime = reference_time + seconds(mean_time_cleaned);

% 3D Plot with date, altitude and wind velocity
figure;
plot3(time_in_datetime,mean_altitude_cleaned,wind_velocity_cleaned,'o
    ')
titleStringOverlook = sprintf('Wind overlook in %s', month);
title(titleStringOverlook)
grid on;
zlabel('Horizontal velocity [m/s]')
ylabel('Altitude [m]')


% 2D Plot with altitude and wind velocity
figure;
plot(mean_altitude_cleaned,wind_velocity_cleaned,'o')
titleStringOverlook = sprintf('Wind velocity in terms of altitude in
    %s', month);
title(titleStringOverlook)
grid on;
ylabel('Horizontal velocity [m/s]')
xlabel('Altitude [m]')

% 2D Plot with longitude, latitude and wind velocity

figure;
scatter(wind_longitude_cleaned, wind_latitude_cleaned, 50,
    wind_velocity_cleaned, 'filled');
cbar = colorbar;
cbar.Label.String = 'Horizontal velocity {m/s]';
xlabel('Longitude');
ylabel('Latitude');
titleStringOverlook = sprintf('Wind speed distribution in %s', month)
    ;
title(titleStringOverlook);
ylabel(colorbar, 'Wind Speed [m/s]');
%-------------------------------
% Create the geographic scatter plot
```

```
182 figure; % Creates a new figure
183 geoscatter(wind_latitude_cleaned, wind_longitude_cleaned, [],
        wind_velocity_cleaned, 'o');
184
185 % Add a colorbar to the figure
186 colorbar;
187
188 % Label the colorbar to indicate what it represents
189 ylabel(colorbar, 'Wind Velocity (units)');
190
191 % Optional: Set the colormap if you want to change the default colors
192 colormap(jet); % This is just an example, MATLAB offers various
        colormaps like 'jet', 'hsv', 'hot', etc.
193
194 % Additional plot settings
195 titleStringOverlook = sprintf('Geographic Distribution of Wind
        Velocity in %s',month);
196 title(titleStringOverlook)
197 grid on; % Turn the grid on for better readabili
198
199 saveas(gcf, fullfile(folderPath, [titleStringOverlook, '.png']), 'png
        ');
200
201 %-------------------------------
202 % 3D Plot with altitude, longitude, wind velocity and altitude
203 figure;
204 scatter3(wind_longitude_cleaned, wind_latitude_cleaned,
        mean_altitude_cleaned, 20, wind_velocity_cleaned, 'filled');
205 titleString3dMap = sprintf('Wind velocity by altitude and position in
         %s', month);
206 xlabel('Longitude');
207 ylabel('Latitude');
208 zlabel('Altitude [m]');
209 title(titleString3dMap);
210 cbar = colorbar;
211 cbar.Label.String = 'Horizontal velocity {m/s]';
212
213 % Create a new figure and set up the map projection using m_map
214 %figure;
215 %m_proj('Miller', 'lat', [-90 90], 'lon', [-180 180]);
216
217 % Plotting the map using m_scatter for scatter plot on the map
218 %m_scatter(wind_longitude_cleaned, wind_latitude_cleaned, 20,
        wind_velocity_cleaned, 'filled');
219 %m_coast('color', 'k'); % Plot coastlines
220
221 % Customize the appearance of the map
222 %m_grid('box', 'fancy', 'tickdir', 'in', 'linestyle', 'none');
223 %m_colorbar;
```

```
224
225 % Add labels and title
226 xlabel('Longitude');
227 ylabel('Latitude');
228 titleStringMap = sprintf('Wind velocity map in %s', month);
229 title(titleStringMap);
230 cbar = colorbar;
231 cbar.Label.String = 'Horizontal velocity {m/s]';
232
233 %  selected your altitude range of interest
234 %min_alt = 11000;
235 %max_alt = 11600;
236 min_alt = 100;
237 max_alt = 500;
238 altitude_range = [min_alt,max_alt];
239
240 k = 1;
241 for i = 1:length(mean_altitude_cleaned)
242
243     if (mean_altitude_cleaned(i) > min_alt && mean_altitude_cleaned(i
    ) < max_alt)
244         matrix_altitude(k,1) = i;
245         matrix_altitude(k,2) = mean_altitude(i);
246         k = k+1;
247     end
248 end
249
250
251 extracted_time = mean_time_cleaned(matrix_altitude(1:end,1));
252
253 extracted_wind = wind_velocity_cleaned(matrix_altitude(1:end,1));
254
255 reference_time = datetime('2000-01-01 00:00:00', 'Format', 'yyyy-MM-
    dd HH:mm:ss', 'TimeZone', 'UTC');
256
257 time_in_datetime = reference_time + seconds(extracted_time);
258
259
260 % Statistics for wind velocity at a defined height
261 mean_wind = mean(extracted_wind);
262 min_wind = min(extracted_wind);
263 max_wind = max(extracted_wind);
264 range_wind = range(extracted_wind);
265 std_wind = std(extracted_wind);
266 stats = {
267     'Mean wind', mean_wind;
268     'Minimum wind', min_wind;
269     'Maximum wind', max_wind;
270     'Range of wind', range_wind;
```

```
271     'Standard deviation', std_wind;
272     };
273
274 titleString = sprintf('Horizontal wind velocity in %s for heights
        between %d and %d meters', month, min_alt, max_alt);
275
276 figure()
277 plot(time_in_datetime,extracted_wind,'o' , time_in_datetime,
        mean_wind*ones(length(time_in_datetime)),'-r');
278 grid on
279 title (titleString)
280 ylabel('horizontal wind velocity (m/s)')
281 xlabel('time')
282 legend('wind measurements','mean value')
283
284 folderPath = 'C:\Users\gabiv\OneDrive\Área de Trabalho\POLITO - Space
        Economy\Thesis\Imagens\MATLAB';
285
286 % Define the edges of the bins for the wind velocity ranges
287 edges = 0:1:25;  % From 0 to 25, with step size of 1
288
289 % Count the number of measurements in each bin
290 [counts, ~] = histcounts(extracted_wind, edges);
291
292 % Total number of measurements
293 total_measurements = numel(extracted_wind);
294
295 % Calculate the percentage for each range
296 percentages = (counts / total_measurements) * 100;
297
298 % Display the results
299 for i = 1:length(edges)-1
300     fprintf('Wind velocity between %d and %d: %d measurements, %.2f%%
        of total\n', ...
301             edges(i), edges(i+1)-1, counts(i), percentages(i));
302 end
```

Bibliography

[1] E. Wrigley. «Energy and the English Industrial Revolution». In: *Philosophical Transactions of the Royal Society A: Mathematical, Physical and Engineering Sciences* 371 (2010). DOI: 10.1098/rsta.2011.0568 (cit. on p. 2).

[2] Data by you. *Map of Oil and Gas Worldwide*. Accessed in November 2023. URL: https://databayou.com/oil/andgas.html (cit. on p. 4).

[3] Dzevad Hadzihafizovic. *Directional drilling on Oil nad Gas field*. Accessed in February 2024. URL: https://www.researchgate.net/publication/378129907_Directional_drilling_on_Oil_nad_Gas_field (cit. on p. 4).

[4] *Renewable Energy by Country*. Accessed: 12/09/2023. 2023. URL: https://wisevoter.com/country-rankings/renewable-energy-by-country/#map (cit. on p. 5).

[5] *Renewable energy generation per country*. Accessed: 12/09/2023. 2023. URL: https://wisevoter.com/country-rankings/renewable-energy-by-country/#map) (cit. on p. 6).

[6] Union of Concerned Scientists. *In-depth details on the 7,560 satellites currently orbiting Earth, including their country of origin, purpose, and other operational details.* Published Dec 8; 2005 Updated May 1, 2023. URL: https://www.ucsusa.org/resources/satellite-database (cit. on p. 7).

[7] European Union Agency for the Space Programme (EUSPA). *2022 Market Report*. https://www.euspa.europa.eu/2022-market-report. Accessed: 15/09/2023. 2022 (cit. on pp. 8, 9).

[8] International Monetary Fund. *GDP, current prices*. 2023. URL: https://www.imf.org/external/datamapper/NGDPD@WEO/OEMDC/ADVEC/WEOWORLD (cit. on p. 9).

[9] Empresa de Pesquisa Energética. *Brazilian Energy Balance 2023*. https://www.epe.gov.br/sites-en/publicacoes-dados-abertos/publicacoes/Paginas/Brazilian-Energy-Balance-2023.aspx. Accessed: 17/09/2023. 2024 (cit. on p. 10).

[10] McKinsey Company. *How to succeed in the expanding global offshore wind market*. https://www.mckinsey.com/industries/electric-power-and-natural-gas/our-insights/how-to-succeed-in-the-expanding-global-offshore-wind-market. Accessed: 01/10/2023. 2022 (cit. on pp. 12, 13).

[11] Orsted. *How do offshore wind turbines work?* Accessed in 2023. URL: https://us.orsted.com/renewable-energy-solutions/offshore-wind/what-is-offshore-wind-power/how-do-offshore-wind-turbines-work (cit. on p. 13).

[12] E.C. Morgan, M. Lackner, R.M. Vogel, and L.G Baise. «Probability distributions for offshore wind speeds». In: 49 (July 2011), pp. 15–25 (cit. on p. 14).

[13] M. Badger, J. Badger, M. Nielsen, C.B. Hasager, and A. Pea. «Wind class sampling of satellite SAR imagery for offshore wind resource mapping». In: 49 (July 2010), pp. 1–18 (cit. on p. 14).

[14] Allan Rodrigues Silva, Felipe Mendonça Pimenta, Arcilan Trevenzoli Assireu, and Maria Helena Constantino Spyrides. «Complementarity of Brazil's hydro and offshore wind power». In: 56 (Dec. 2015), pp. 2–15 (cit. on p. 14).

[15] Mario Orestes Aguirre Gonzalez, Andressa Medeiros Santiso, David Cassimiro de Melo, and Rafael Monteiro de Vasconcelos. «Regulation for offshore wind power development in Brazil». In: 145 (Aug. 2020), pp. 3–7 (cit. on p. 15).

[16] Siemens Gamesa Renewable Energy. *SSG 11.0-200 DD Offshore wind turbine*. Siemens Gamesa Renewable Energy. Aug. 2023. URL: https://www.siemensgamesa.com/products-and-services/offshore/wind-turbine-sg-11-0-200-dd (cit. on p. 22).

[17] van den Anke Berg. «Wind turbine power and sound in relation to atmospheric stability». In: *Wind Energy* 11 (2008), pp. 151–169. DOI: 10.1002/WE.240 (cit. on pp. 28, 29).

[18] Amanda Ribeiro de Andrade, Victor F. M. B. Melo, Daisy Beserra Lucena, and R. Abrahão. «Wind speed trends and the potential of electricity generation at new wind power plants in Northeast Brazil». In: *Journal of the Brazilian Society of Mechanical Sciences and Engineering* 43 (2021). DOI: 10.1007/s40430-021-02911-y (cit. on pp. 30, 37–41).

[19] Vaishali Sohoni, S. Gupta, and R. Nema. «A Critical Review on Wind Turbine Power Curve Modelling Techniques and Their Applications in Wind Based Energy Systems». In: *Journal of Energy* 2016 (2016), pp. 1–18. DOI: 10.1155/2016/8519785 (cit. on p. 30).

[20] Hongyang Dong, Jingjie Xie, and Xiaowei Zhao. «Wind farm control technologies: from classical control to reinforcement learning». In: *Progress in Energy* 4 (2022). DOI: 10.1088/2516-1083/ac6cc1 (cit. on p. 32).

[21] *Wake Effect Model*. Accessed: 15/11/2023. 2023. URL: https://www.wasp.dk/software/wasp/wake-effect-model (cit. on p. 31).

[22] A. Ikpe and Ekom Etuk Mike. «3 Dimensional Modelling of the Wind Flow Trajectories and Its Characteristic Effects on Horizontal Axis Wind Turbine Performance at Different Wind Regimes». In: *Journal of International Environmental Application and Science* 15 (2019), pp. 68–80 (cit. on p. 34).

[23] Aviation Safety. *Surviving wind shear*. August, 2022. URL: https://www.aviationsafetymagazine.com/airmanship/surviving-windshear/ (cit. on p. 35).

[24] J. D. Kooning, T. Vandoorn, J. V. D. Vyver, B. Meersman, and L. Vandevelde. «Shaft speed ripples in wind turbines caused by tower shadow and wind shear». In: *Iet Renewable Power Generation* 8 (2014), pp. 195–202. DOI: 10.1049/IET-RPG.2013.0008 (cit. on p. 36).

[25] Kamran Shirzadeh, H. Hangan, C. Crawford, and Pooyan Hashemi Tari. «Investigating the loads and performance of a model horizontal axis wind turbine under reproducible IEC extreme operational conditions». In: 6 (2021), pp. 477–489. DOI: 10.5194/WES-6-477-2021 (cit. on p. 36).

[26] CEPEL – Electric Energy Research Center (Centro de Pesquisa de Energia Elétrica. «Atlas of Brazilian Wind Potential: Simulations 2013 (Atlas do Potencial Eólico Brasileiro: Simulações 2013)». In: (2013) (cit. on p. 37).

[27] H. Camelo, P. Carvalho, João Verçosa Leal Junior, and J. A. P. Filho. «Análise estatística da velocidade de vento do estado do Ceará». In: 29 (2008). DOI: 10.5020/23180730.ANO.PI (cit. on p. 37).

[28] Instituto Brasileiro de Geografia e Estatística. *Censo 2022*. 2023. URL: https://censo2022.ibge.gov.br/panorama/ (cit. on p. 42).

[29] U.S. Department of Energy. *Wind Turbines: Bigger and Better*. 2023. URL: https://www.energy.gov/eere/articles/wind-turbines-bigger-better (cit. on p. 47).

[30] WeatherSpark. *Clima característico em Santos, Brasil durante o ano*. Accessed in 2024. URL: https://pt.weatherspark.com/y/30272/Clima-caracter%C3%ADstico-em-Santos-Brasil-durante-o-ano (cit. on pp. 47, 49).

[31] CanalEnergia. *Preços do A-5 variam de R$ 194,96/MWh a mais de R$ 600/MWh*. insira o ano. URL: https://canalenergia.com.br/noticias/53221995/precos-do-a-5-variam-de-r-19496mwh-a-mais-r-600mwh (cit. on p. 55).